Effects of fat particles on the stability of complex food systems

Tomohito Hanazawa

2019

Effects of fat particles on the stability of complex food systems

Contents

Chapter 1

General Introduction

Most of food is a complex or multi-component system. In many types of food, various components such as proteins, polysaccharides and lipids are not solubilized, but dispersed as an assembled form in water existing as a continuous phase. In the case of dairy foods, basic components are milk proteins, lactose, minerals and milk fats, but other ingredients such as polysaccharides, surfactants and vegetable fats are added in accordance with the various requirements by industries and consumers. Furthermore, when whipped cream and ice cream are produced, air bubbles are also incorporated into the system as the new dispersed phase. Therefore, a large number of dairy foods with diverse dispersed phases are commercially available. It is of great importance, which components should be selected and combined, what kind of equipment should be used for the production, and how the processed conditions should be optimized, in order to impart the high quality to dairy food products. The long-term stability with respect to colloidal dispersions is also required to assure the shelf life of dairy food products. In this context, the destabilization phenomena such as creaming and flocculation of fat particles, phase separation into protein-rich or polysaccharide-rich regions, and flotation and disappearance of bubbles, etc., are often objects for fundamental and applied studies on quality evaluation and quality control of dairy food products.

Phase separation has been observed on caseins (including sodium caseinate) + polysaccharide systems (Bourriot, Garnier, & Doublier, 1999a,b; Hamar, Tamehana, Munro, & Singh, 2001; Maroziene & de Kruif, 2000; Tuinier & de Kruif, 1999). Such phase separation is a consequence of depletion flocculation phenomena, as described in the following papers (Syrbe, Bauera, & Klostermeyer, 1998; Tuinier, & de Kruif, 1999).

A difference in polysaccharide concentration between the inter-protein region and the outside region surrounding proteins molecules causes a difference in the osmotic pressure between two regions, thereby expelling water from the inter protein region and increasing attractive force to associate protein molecules (Fig. 1-1). According to the progress of protein aggregation, two aqueous phase, that is, protein-rich phase and polysaccharide-rich phase are formed and segregated from each other. Either protein-rich phase or polysaccharide-rich phase disperses in another one to form so-called water-in-water (W/W) emulsion (Fig. 1-2 (b)). The W/W emulsions finally leads to the phase separation (Fig. 1-2 (c)).

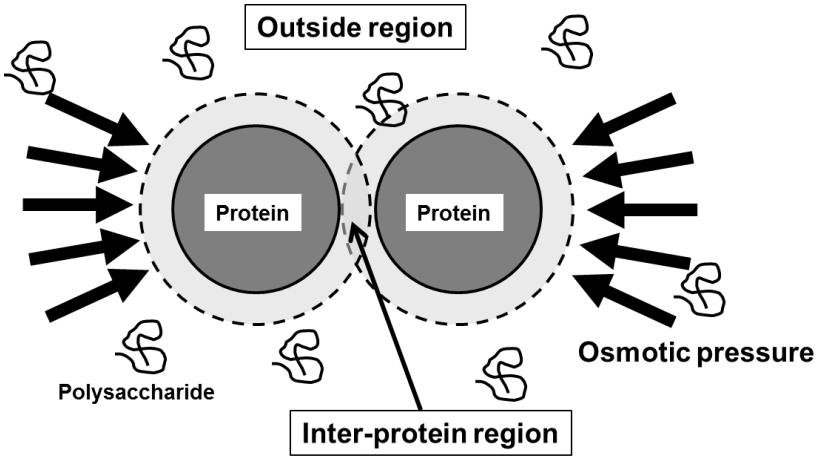

Fig. 1-1. Description of depletion flocculation in the protein–polysaccharide mixture.

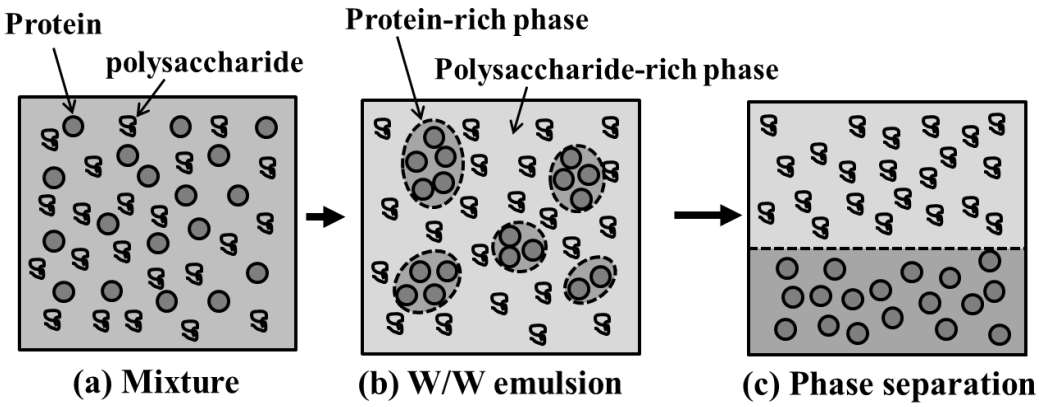

Fig. 1-2. Schematic representation of phase separation process of the protein–polysaccharide mixture.

Recently, several studies have shown that added particles in a phase-separating system can adsorb onto the interface between two aqueous phases and form viscoelastic particle layer (Araki & Tanaka, 2006; Kim, Stratford, Adhikari, & Cates, 2008; Stratford, Adhikari, Pagonabarraga, Desplat, & Cates, 2005). Computer simulation also proposed such structures – bicontinious interfacially jammed emulsion gels, "bijels" (Cates & Clegg, 2008) (Fig. 1-3). In a protein (gelatin) + polysaccharide (starch) system, accumulation of colloidal particles at the water–water interface was observed, which affected the complex bicontinuous microstructure of protein-rich phase and polysaccharide-rich phase and the dynamics of phase separation (Firoozmand, Murray, & Dickinson, 2009). These studies suggest that colloidal particle can contribute to stability of phase-separating system of foods. As described above, many dairy foods include fat particles. However, the effect of fat particles on the phase separation of dairy food system have been scarcely investigated.

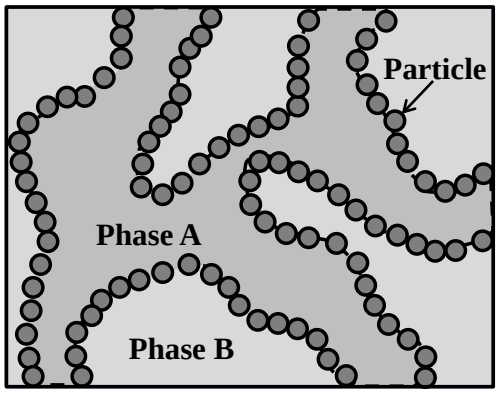

Fig. 1-3. Typical image of bicontinious inter facially jammed emulsion gels, "bijels"**.**

For whipped cream, air is incorporated into the system to create newly the air–water interface during the whipping process, and the adsorption of fat particles onto the air-water interface should be investigated with respect to the formation and stabilization of whipped state. The mixture including air bubbles is particularly unstable,

because air bubbles melt easily into water. To avoid Ostwald ripening between bubbles in food, quick forming of the firm interfacial membrane is needed (Dickinson, 1992). Anderson & Brooker (1988) revealed that fat particles accumulate at the air–water interface and compose the interfacial structure in whipped cream by electron microscopy. The typical whipping process of dairy cream consists of three steps (Anderson & Brooker, 1988; Besner & Kessler, 1998; Fredrick et al., 2013; Hotrum, Cohen Stuart, van Vliet, Avino, & can Aken, 2005, Jakubczyk & Niranjan, 2006; Needs & Huitson, 1991; Noda & Shiinoki, 1986; van Aken, 2001) (Fig. 1-4).

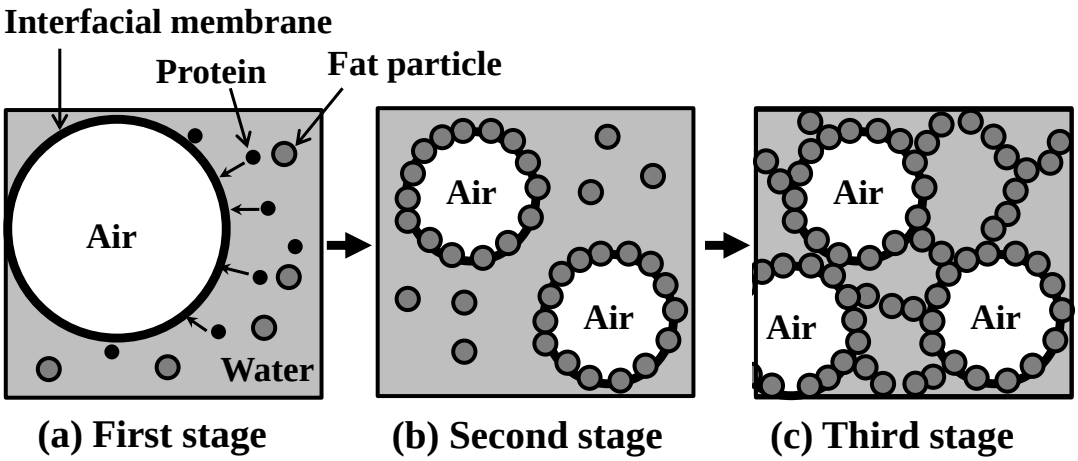

Fig. 1-4. Schematic representation of whipping process of dairy cream.

First, a protein membrane forms at air–water interface. After the large bubbles form through whipping, proteins adsorbed at the newly-produced air–water interface. In the second stage, the large bubbles are further sheared to produce small bubbles, by spreading the area of the air–water interface. The newly-formed interfacial membrane mainly consists of fat particles or their aggregates. In the third stage, a network structure including bubbles via fat particle at air–water interface causes viscosity and firmness of whipped cream. Thus, it is important to elucidate the process of the fat particle adsorption and the interfacial structure formation.

In actual food products, fat or oil vary in fatty acid composition greatly, and fat crystallization occurs according to temperature. The solid fat content (SFC) in fat particles has a great impact on their aggregation via partial coalescence (Boode & Walstra, 1993). If fat particles contain some amount of fat crystals, the particles can be connected to eachother via the fat crystals (Fig. 1-5). It is called partial coalescence. There are several papers demonstrating that such partial coalescence is maximised when the SFC is in the range of approximately 10–50% (Boode & Walstra, 1993; Davies, Dickinson, & Bee, 2000; Hinrichs & Kessler, 1997; Mutoh, Nakagawa, Noda, Shiinoki, & Matsumura, 2001; Needs & Huitson, 1991).

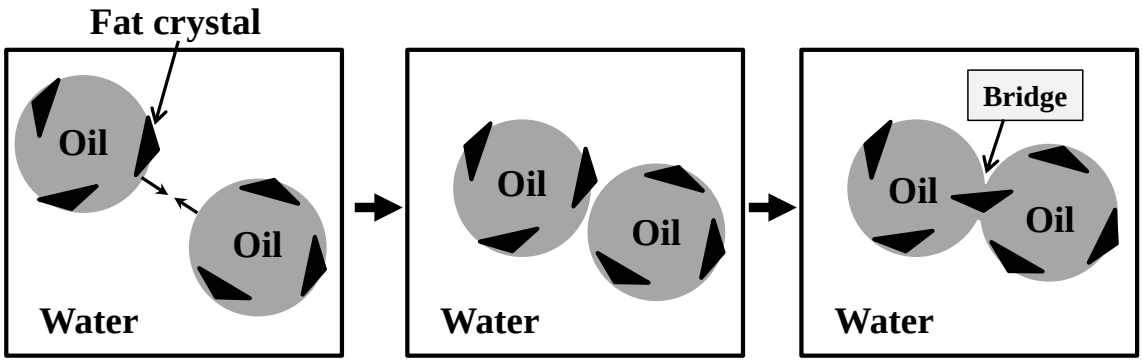

Fig. 1-5. Schematic representation of partial coalescence mechanism caused by fat crystal.

In this thesis, I studied the adsorption behaviour of fat particle with varying SFC at the water–water interface and air–water interface of dairy food models. In chapter 2, the phase separation behaviour of xanthan + sodium caseinate was observed as function of these two variables with different pH and Ca^{2+} concentration, and then the effects of addition of oil (n-tetradecane) droplets emulsified by sodium caseinate on the phase separation behaviour of this binary macromolecular systems was investigated. In chapter 3, my interest was how the soild/liquid composition in oil droplets affects the

efficacy of oil droplets addition on the prevention of phase separation of the xanthan + sodium caseinate mixtures. I formulated the solid/liquid composition of emulsified oil droplets using n-tetradecane (TD) as liquid oil and eicosane (EC) as solid fat. In this chapter, interfacial viscosity at the interface between xanthan rich phase and sodium caseinate rich phase was also measured under the oil droplet addition to know the relation between mechanical strength of interface and the stability of two aqueous phases. In chapter 4, assuming the application to whipped cream, the adsorption of emulsified fat particles in creams onto the air–water interface was investigated. Three creams were prepared by mixing sodium caseinate solutions and 3 vegetable oils with different SFC profile, respectively. The effects of SFC in fat particles on their adsorption behaviour at the air–water interface was examined by using interfacial tension and rheology measurement technique.

References

Anderson, M., & Brooker, B. E. (1988). Dairy Foams. In E. Dickinson & G. Stainsby, (Eds.), *Advances in food emulsions and foams*. (Chapter 5, pp. 221–255). London, UK: Elsevier Applied Science.

Araki, T., & Tanaka, H. (2006). Wetting-induced depletion interaction between particles in a phase-separating liquid mixture. *Physical Review E, 73,* 061506.

Besner, H., & Kessler, H. G. (1998). Interfacial interaction during the foaming of nonhomogenized cream. *Milchwissenschaft, 53,* 682–686.

Boode, K., & Walstra, P. (1993) Kinetics of partial coalescence in oil-in-water emulsions. In E. Dickinson & P. Walstra, (Eds.), *Food colloids and polymers: Stability and mechanical properties*. (pp. 23–30). Cambridge, UK: Royal Society of Chemistry.

Bourriot, S., Garnier, C., & Doublier, J.-L. (1999a). Micellar-casein-κ-carrageenan mixtures. I. Phase separation and ultrastructure. *Carbohydrate Polymers, 40,* 145–157.

Bourriot, S., Garnier, C., & Doublier, J.-L. (1999b). Phase separation, rheology and microstructure of micellar casein-guar gum mixtures. *FoodHydrocolloids*, *13,* 43–49.

Cates, M. E., & Clegg, P. S. (2008). Bijels: a new class of soft materials. *Soft Matter*, *4*, 2132–2138.

Davies, E., Dickinson, E., & Bee, R. (2000). Shear stability of sodium caseinate emulsions containing monoglyceride and triglyceride crystals. *Food Hydrocolloids, 14,* 145–153.

Dickinson, E. (1992). *An introduction to food colloids*. Oxford, UK: Oxford University Press.

Firoozmand, H., Murray, B. S., & Dickinson, E. (2009). Interfacial structuring in a phase-separating mixed biopolymer solution containing colloidal particles. *Langmuir*,

25, 1300–1305.

Fredrick, E., Heyman, B., Moens, K., Fischer, S., Verwijlen, T., Moldenaers, P., … & Dewettinck, K. (2013). Monoacylglycerols in dairy recombined cream: II. The effect on partial coalescence and whipping properties. *Food Research International, 51,* 936–945.

Goff, H. D. (1997). Instability and Partial Coalescence in Whippable Dairy Emulsions. *Journal of Dairy Science, 80,* 2620–2630.

Hamar, Y., Tamehana, M., Munro, P. A., & Singh, H. (2001). Viscosity, microstructure and phase behavior of aqueous mixtures of commercial milk protein products and xanthan gum. *Food Hydrocolloids*, *15*, 565–574.

Hinrichs, J., & Kessler, H. G. (1997). Fat content of milk and cream and effects on fat globule stability. *Journal of Food Science, 62,* 992–995.

Hotrum, N. E., Cohen Stuart, M. A. C., van Vliet, T., Avino, S. F., & van Aken, G. A. (2005). Elucidating the relationship between the spreading coefficient, surface-mediated partial coalescence and the whipping time of artificial cream. *Colloids and Surfaces A: Physicochemical and Engineering Aspects, 260,* 71–78.

Jakubczyk, E. & Niranjan, K. (2006). Transient development of whipped cream properties. *Journal of Food Engineering, 77,* 79–83.

Kim, E., Stratford, K., Adhikari, R., & Cates, M. E. (2008). Arrest of fluid demixing by nanoparticles: a computer simulation study. *Langmuir*, *24*, 6549–6556.

Maroziene, A., & de Kruif, C. G. (2000). Interaction of pectin and casein micelles. *Food Hydrocolloids*, *14*, 391–394.

Mutoh, T.-A., Nakagawa, S., Noda, M., Shiinoki, Y., & Matsumura, Y. (2001). Relationship between characteristics of oil droplets and solidification of thermally treated cream. *Journal of the American Oil Chemists' Society, 78,* 177–183.

Needs, E. C., & Huitson, A. (1991). The contribution of milk serum-proteins to the development of whipped cream structure. *Food Structure, 10,* 353–360.

Noda, M., & Shiinoki, Y. (1986). Microstructure and rheological behavior of whipping cream. *Journal of Texture Studies, 17,* 189–204.

Stratford, K., Adhikari, R., Pagonabarraga, I., Desplat, J.-C., & Cates, M. E. (2005). Colloidal jamming at interfaces: a route to fluid-bicontinuous gels. *Science, 309*, 2198–2201.

Syrbe, A., Bauera,W. J., & Klostermeyer, H. (1998). Polymer science concepts in dairy systems - an overview of milk protein and food hydrocolloid interaction. *International Dairy Journal, 8,* 179–193.

Tuinier, R., & de Kruif, C. G. (1999). Phase behaviour of casein micelles/exocellular polysaccharide mixtures: experiment and theory. *Journal of Chemical Physics*, *110*, 9296–9304.

Van Aken, G. A. (2001). Aeration of emulsions by whipping. *Colloids and Surfaces A: Physicochemical and Engineering Aspects, 190*, 333–354.

Chapter 2

The influence of oil droplets on the phase separation of protein–polysaccharide mixtures

2.1. Introduction

Dairy protein, polysaccharides and oil are the main components of many food products. Therefore, it is important to understand the interactions between these components in order to control the stability of existing products and for the development of novel foods. Casein is the main protein component of milk and is composed of four principal proteins: α_{s1}-casein, α_{s2}-casein, β-casein and κ-casein. The caseins are associated with calcium phosphate in the form of colloidal particles known as casein micelles (Dickinson, 2006). Sodium caseinate is widely used as an emulsifying agent in many dairy products and is manufactured by removing calcium phosphate from milk casein through acidification, precipitation and neutralization with alkali, which destroys much of the native casein structure although subunits of this structure seem to persist (sometimes referred to as sub-micelles). Polysaccharides are used to control the texture and stability of products and xanthan gum is one such example. Xanthan exhibits strongly pseudoplastic flow properties in solution even at low concentrations (Moschakis, Murray, & Dickinson, 2005) and is used to prevent sedimentation or creaming of particles under quiescent or low shear conditions, whilst still allowing pumping, mixing etc., under high shear. Oil is a component of many foods, where it imparts or carries important flavour and aroma components as well as important nutrients. Since the bulk of most foods is aqueous, oil is most frequently present or incorporated as oil-in-water (O/W) emulsions, often stabilized by proteins such as sodium caseinate.

Complex interactions between these different components can occur which alter their stabilizing effects. For example, the proteins and polysaccharides may not be compatible and phase separation into protein-rich and polysaccharide-rich phases, or protein–polysaccharide coacervation, may occur (Doublier, Garnier, Renarda, & Sanchez, 2000; Syrbe, Bauera, & Klostermeyer, 1998; Tuinier & de Kruif, 1999). Indeed, phase separation has been observed in various casein(ate) + polysaccharide systems (Bourriot, Garnier, & Doublier, 1999a,b; Maroziene & de Kruif, 2000; Tuinier & de Kruif, 1999), depending upon the solution conditions, i.e., biopolymer concentrations, pH, ionic composition, etc. For example, Hamar, Tamehana, Munro, and Singh (2001) observed that phase separation did not occur in sodium caseinate + xanthan mixtures at neutral pH, although skim milk + xanthan and milk protein concentrate + xanthan mixtures did phase separate. Perrechil and Cunha (2012) showed that sodium caseinate + locust bean gum mixtures exhibited no phase separation at pH 7.0, but acidification to pH 5.5 led to phase separation, depending on the composition. Similarly, phase separation of casein + guar gum mixtures appears to be dependent on both pH and ionic strength, phase separation only being observed at ionic strengths above 0.09–0.2 mol dm^{-3} at neutral pH (Antonov, Lefebvre, & Doublier, 1999).

In addition, biopolymers may cause depletion flocculation of oil droplets. For example, the microstructure and stabilization of a sodium caseinate-stabilized 30 vol% O/W emulsion changed considerably due to the presence of polysaccharide xanthan (Dickinson, 2006; Moschakis et al., 2005, 2006). There it was concluded that the ‘stabilizing’ effect of xanthan was an indirect consequence of depletion flocculation of the droplets, leading to a mechanically stable protein + droplet-rich network surrounded by a xanthan-rich phase.

Previous studies have also shown that the phase separation of mixtures can be influenced by the presence of particles. The self-assembly of colloidal particles in a phase-separating system has the potential to arrest the process of de-mixing arising from

spinodal decomposition (or nucleation and growth) by the formation of a viscoelastic particle layer at the liquid–liquid interface (Araki & Tanaka, 2006; Cates & Clegg, 2008; Kim, Stratford, Adhikari, & Cates, 2008; Stratford, Adhikari, Pagonabarraga, Desplat, & Cates, 2005). These structures - bicontinuous interfacially jammed emulsion gels, or "bijels", were first proposed on the basis of computer simulation (Cates & Clegg, 2008). In a protein (gelatin) + polysaccharide (starch) system, accumulation of colloidal particles at the water–water interface was observed which seemed to change the nature of the microstructure and the dynamics of the phase separation (Firoozmand, Murray, & Dickinson, 2009). The effects were observed with polystyrene latex particles but also with small (<1 μm) emulsion droplets acting as particles. The phase type of multiple emulsions has also been shown to depend on the ratio of oil, protein and polysaccharide (Perrechil & Cunha, 2012).

In this work a model system consisting of sodium caseinate + xanthan ± a low volume fraction of oil-in-water emulsion droplets was studied, with the aim of discovering what effects the droplets have on the macroscopic and microscopic phase separation of the system. However, since the aggregation of sodium caseinate is well known to depend on pH and calcium ion concentration ($[Ca^{2+}]$), to start with the phase separation behaviour of xanthan + sodium caseinate was investigated as function of these two variables, followed by experiments on the same systems where oil droplets were included.

2.2. Materials and methods

2.2.1. Materials

Spray-dried sodium caseinate (82% w/w dry protein, 6% w/w moisture, 6% w/w fat and ash) was supplied by DMV International (Veghel, Netherlands). The calcium concentration of the sodium caseinate (SC) sample was determined by atomic absorption as 0.78 mg g^{-1}. A food-grade xanthan gum powder (Keltrol, product code

0F8209A) was obtained from CP Kelco UK, Surrey, UK. The oil for emulsions was *n*-tetradecane (99%) (from Alfa Aesar, Heysham, UK) or 1-bromohexadecane (from Sigma–Aldrich, Gillingham, UK). AnalR grade sodium azide, $CaCl_2 \cdot H_2O$, glucono-δ-lactone (GDL), imidazole, sodium hydroxide, hydrochloric acid, sodium acetate were also obtained from Sigma–Aldrich (Gillingham, UK) as were Nile Red and Nile Blue dyes for confocal microscopy. Water purified by treatment with a Milli-Q apparatus (Millipore, Bedford, UK), with a resistivity not less than 18.2 MΩ cm was used for the preparation of all aqueous solutions. Sodium azide was added to all aqueous solution at 0.02% w/w as an anti-microbiological agent.

2.2.2. Mixture preparation

SC stock solutions were prepared by dispersing the protein (6.25% w/w) in water by gentle stirring for 1 h. The $[Ca^{2+}]$ in protein stock solutions was adjusted to between 1 and 64 mM by addition of $CaCl_2 \cdot H_2O$ solution. The pH of the SC solutions was adjusted (generally to pH 6.4, 5.9 or 5.4) by addition of 0.1 mol dm^{-3} NaOH or GDL. Stock solutions with GDL were kept at ambient temperature overnight to decrease the pH. In the final SC solutions, the SC concentration was 5% w/w. Stock solutions of 2% w/w xanthan at pH 6.4, 5.9 and 5.4 were prepared by dispersing the gum in either 0.02 M acetate buffer (pH 5.4) or imidazole buffer (pH 6.4 or pH 5.9) with gentle stirring and kept overnight in a refrigerator before use. A 2.5% w/w SC solution was prepared in pH 6.4 imidazole buffer as an emulsifier. Oil-in-water (O/W) emulsions were prepared using a jet homogenizer (Burgaud, Dickinson, & Nelson, 1990) operating at 300 ± 20 bar at ambient temperature. In the final emulsion, the SC concentration was 2% (w/v) and the concentration of dispersed oil phase was 20 vol%. Mixtures of SC + xanthan or SC + xanthan + emulsion were prepared in 7 ml glass vials (Ø 23 mm × H 34 mm, from VWR International Ltd, UK) and mixed by an Ultra Turrax T25 homogenizer (IKA–Werke GmbH & Co., Germany) at 9500 rpm at room

temperature for 3 min. The [Ca^{2+}] was adjusted by addition of $CaCl_2 \cdot H_2O$. Any bubbles that formed during mixing were destroyed by brief bursts of ultrasound from an ultrasonic probe (Vibra-Cell VC 130, Sonics & Materials, Inc., Newtown, USA). This was to ensure that, as far as possible, bubbles did not obscure the boundaries of the different phases that formed subsequently, or became trapped within these phases.

2.2.3. Determination of phase separation

Phase diagrams for SC + xanthan were obtained by making a large number of samples at different SC concentration ([SC]), xanthan concentration ([xanthan]), [Ca^{2+}] and pH in the 7 ml glass vials. The samples were kept for 24 h at room temperature and phase separation detected by visual observation.

2.2.4. Confocal microscopy

A Leica TCS SP2 confocal laser scanning microscope (CLSM) was used, mounted on a Leica Model DM REX microscope base. A 40× oil-immersion objective with numerical aperture 1.25 was used. The CLSM was operated in fluorescence mode using Nile Red dye to stain the oil phase. A staining solution of concentration 0.01% (w/v) was prepared by dissolving 0.001 g of Nile Red in 10 ml of 1,2-propanediol. Protein was stained with Nile Blue. A staining solution of concentration 0.01% (w/v) was prepared by dissolving 0.001 g of Nile Blue in 10 ml of MilliQ water. These solutions were stored in a dark place before use. Fluorescence from Nile Red in the oil was excited with the 488 nm laser line, fluorescence from Nile Blue (protein-rich regions) was excited with the 633 nm laser line, whereas regions rich in just xanthan and not protein were assumed as dark (i.e., non-fluorescent) in the micrographs. Five minutes after preparation, samples of approximately 3 ml were transferred to a small vessel and mixed with 30 μl of the Nile Red and/or Nile Blue dye solutions by shaking by hand. The sample was then immediately placed into a welled slide 30 mm diameter

and 0.3 mm in depth. A cover slip (0.17 mm thickness) was placed on top of the well. Micrographs started to be recorded 30 μm below the cover slip approximately 10 min after the mixture preparation.

2.2.5. Particle size distributions of sodium caseinate

5% w/w SC solutions at pH 6.4, 5.9, and 5.4 were prepared. These stock solutions were diluted to 0.5% w/w SC by addition of $CaCl_2$ solutions in buffer such that the final [Ca^{2+}] was 0-40 mM. The solutions were filtered through a 1.0 μm filter (Puradisc 25, Whatman, Little Chalfont, UK) except those at pH 5.9 and [Ca^{2+}] >30 mM, or pH 5.4 and [Ca^{2+}] >10 mM. These latter two solutions could not be filtered because they caused the blockage of the filters. Particle size distributions of the SC solutions were then determined using a Malvern Zetasizer Nano-ZS (Malvern Instruments Ltd, UK), using a refractive index of 1.570 for SC (Mimouni, Deeth, Whittaker, Gidley, & Bhandari, 2009) and 1.330 for the dispersion medium (i.e., water). The absorbance of proteins was assumed = 0.001.

2.2.6. Particle size distributions of the emulsions

Particle distributions of emulsions were measured via a Malvern Mastersizer Hydro 2000 (Malvern Instruments Ltd, UK). For all emulsions the refractive index of oil droplets was taken as 1.460 (*n*-tetradecane) and that of the dispersion medium 1.330. The absorbance of proteins was assumed = 0.001. For the stock SC-stabilized emulsion the mean droplet diameter d_{32} = 0.36 μm. For examination of the effects of pH and [Ca^{2+}] on droplet size, samples of the stock emulsion (20 vol.%) were diluted to 10 vol.% by addition of $CaCl_2$ solutions in the appropriate buffer, to give [Ca^{2+}] between 15 and 40 mM. These samples were kept in glass vessel for up to 10 days at 20 °C. After shaking gently, particle distributions of these samples were measured.

2.3. Results and discussion

2.3.1. Phase diagrams of sodium caseinate + xanthan mixtures

As usual, square brackets denote concentrations in the following description of the results. Fig. 2-1(a) shows the phase diagram at pH 6.4. Phase separation was not observed in the mixtures for [Ca^{2+}] <20 mM. Above 20 mM [Ca^{2+}] at least 1.5% w/w

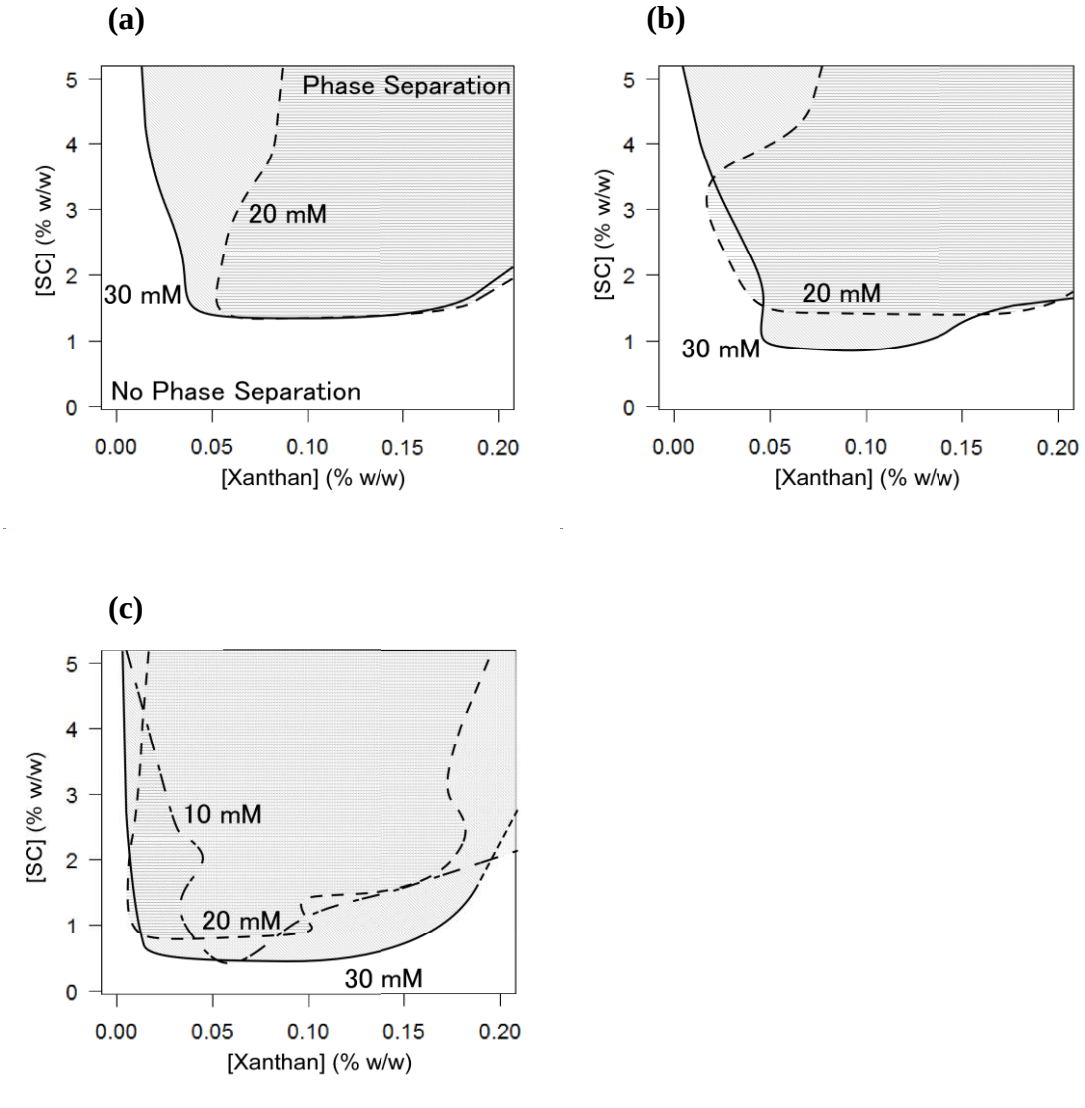

Fig. 2-1. Phase diagrams of SC + xanthan mixtures at various pH and [Ca^{2+}]: (a) pH 6.4; (b) pH 5.9; and (c), pH 5.4: Solid line, [Ca^{2+}] = 30 mM; dashed line, [Ca^{2+}] = 20 mM; dashed dotted line, [Ca^{2+}] = 10 mM. Regions above the lines promote phase separation.

SC and 0.05% w/w xanthan were needed to effect phase separation, whilst for [SC] > 4% w/w, more than 0.07% w/w xanthan was needed. For [Ca^{2+}] = 30 mM, phase separation occurred above 1.5% w/w SC, similar to the situation with 20 mM [Ca^{2+}] but the two phase region extended to lower [xanthan]. Fig. 2-1(b) shows the phase diagram at pH 5.9. Phase separation was not observed in the mixtures for [Ca^{2+}] < 20 mM, as in the mixtures at pH 6.4, but compared to pH 6.4, the 2-phase region was expanded into slightly lower [SC] and [xanthan] at [Ca^{2+}] = 20 mM, whilst at [Ca^{2+}] = 30 mM, the phase-separated region extended to even lower [SC]. Fig. 2-1(c) shows the phase diagram at pH 5.4, where the two-phase region is extended to even lower [xanthan] and [SC] at 20 or 30 mM [Ca^{2+}] compared to pH 5.9, with phase separation now occurring at 10 mM [Ca^{2+}].

Fig. 2-2 is derived from the same data, but shows the phase diagram at a fixed [SC] = 3% w/w as function of [Ca^{2+}]. It shows even more clearly how pH and [Ca^{2+}] affect phase separation: at higher [Ca^{2+}] and/or lower pH, phase separation is even more

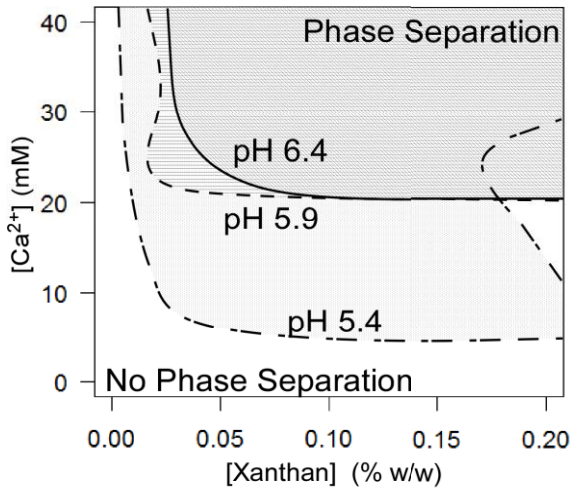

Fig. 2-2. Phase diagram of SC + xanthan mixtures containing 3% w/w SC as function of [Ca^{2+}]: Solid line, pH 6.4; dashed line, pH 5.9; dashed dotted line, pH 5.4. Regions above the lines promote phase separation.

likely to occur at a given [xanthan]. This might be expected, as lower pH and/or [Ca^{2+}] drive aggregation of the SC, and larger aggregates of SC are even less likely to mix with the xanthan.

2.3.2. Effect of oil droplets on the phase separation

Fig. 2-3 shows the effects of adding up to 3% w/w of oil droplets on the volumes of the different phases that separate for [SC] = 2, 3 and 4% w/w, at a fixed [xanthan] = 0.1% w/w and pH 6.4, for [Ca^{2+}] = 10, 22 or 32 mM. The two major phases (by volume) that appeared were a lower SC-rich phase and above it a xanthan-rich phase. Sometimes a third, droplet-rich region appeared above the xanthan-rich phase, but this was much smaller in volume. At [Ca^{2+}] = 10 mM (Fig. 2-3(a)-(c)), virtually no separation of the SC + xanthan occurred, although at the higher [SC] a very low volume upper droplet phase was visible. At [Ca^{2+}] = 22 mM (Fig. 2-3(d)-(f)), increasing the volume fraction of oil droplets clearly seemed to suppress the appearance of separate SC- and xanthan-rich phases, but at the expense of a thin upper droplet-rich phase appearing. However, at [Ca^{2+}] = 32 mM (Fig. 2-3(g)-(h)), this suppression seemed to be curtailed at [SC] = 2% w/w and was completely absent at [SC] = 3 or 4% w/w.

Fig. 2-4 show similar effects to those observed in Fig. 2-3, but at different [xanthan] at pH 6.4 and different [SC] and [Ca^{2+}]. The results again show that suppression of phase separation of the SC and xanthan appears to be produced by the addition of oil droplets, although they are less effective at this when the driving force for phase separation is stronger, i.e., at higher [SC] and/or [Ca^{2+}].

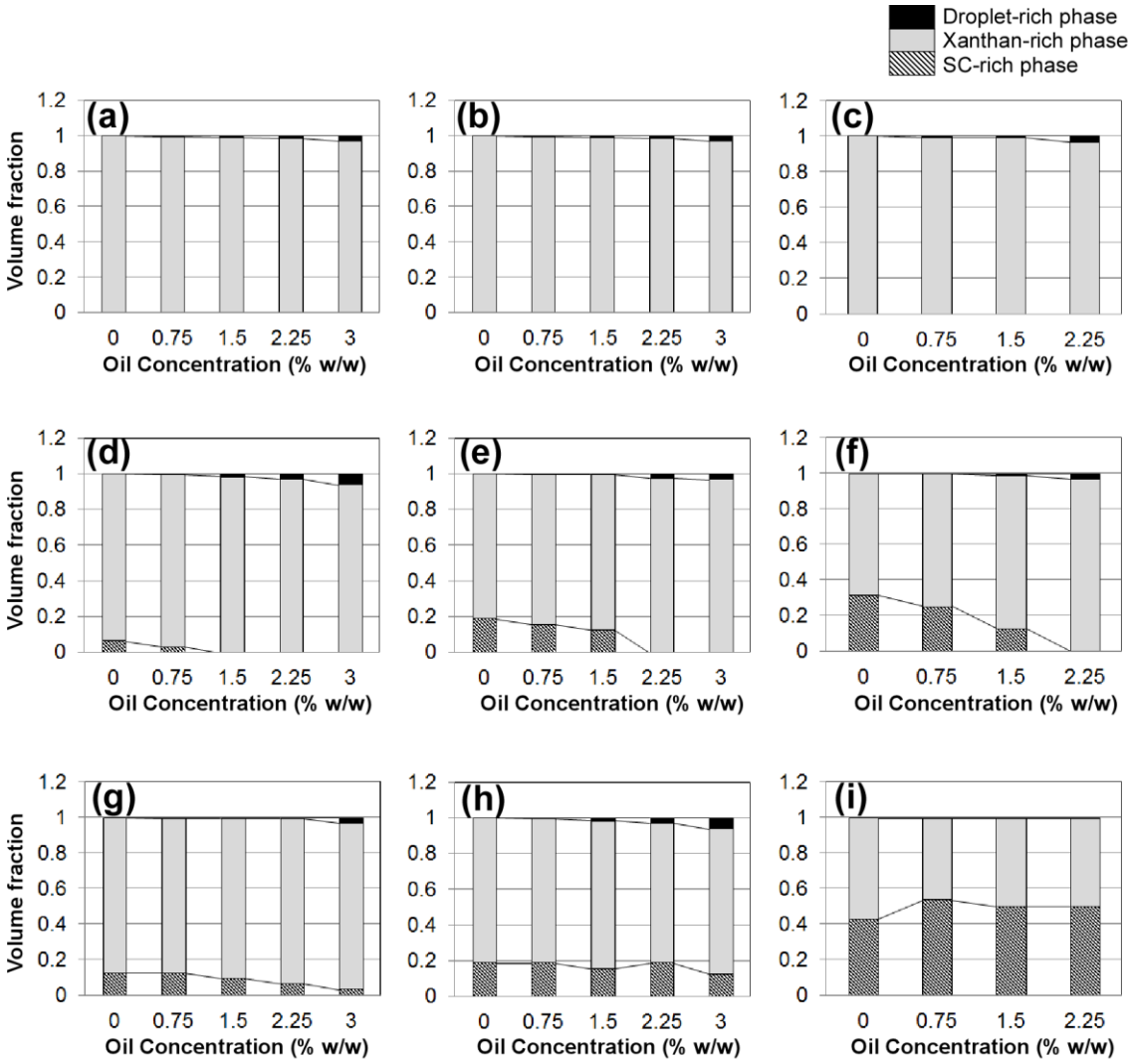

Fig. 2-3. Volume fraction of different phases of SC + xanthan mixtures containing 0.1% w/w xanthan at pH 6.4 at various [Ca^{2+}] as a function of weight % added oil droplets: 2% w/w SC (a), (d) and (g); 3% w/w SC (b), (e) and (i); 4% w/w SC (c), (f) and (i); [Ca^{2+}] = 10 mM (a-c); [Ca^{2+}] = 22 mM (d-f); [Ca^{2+}] = 32 mM (g-i). Black = upper droplet-rich phase, light grey = xanthan-rich phase; hatched = lower SC-rich phase.

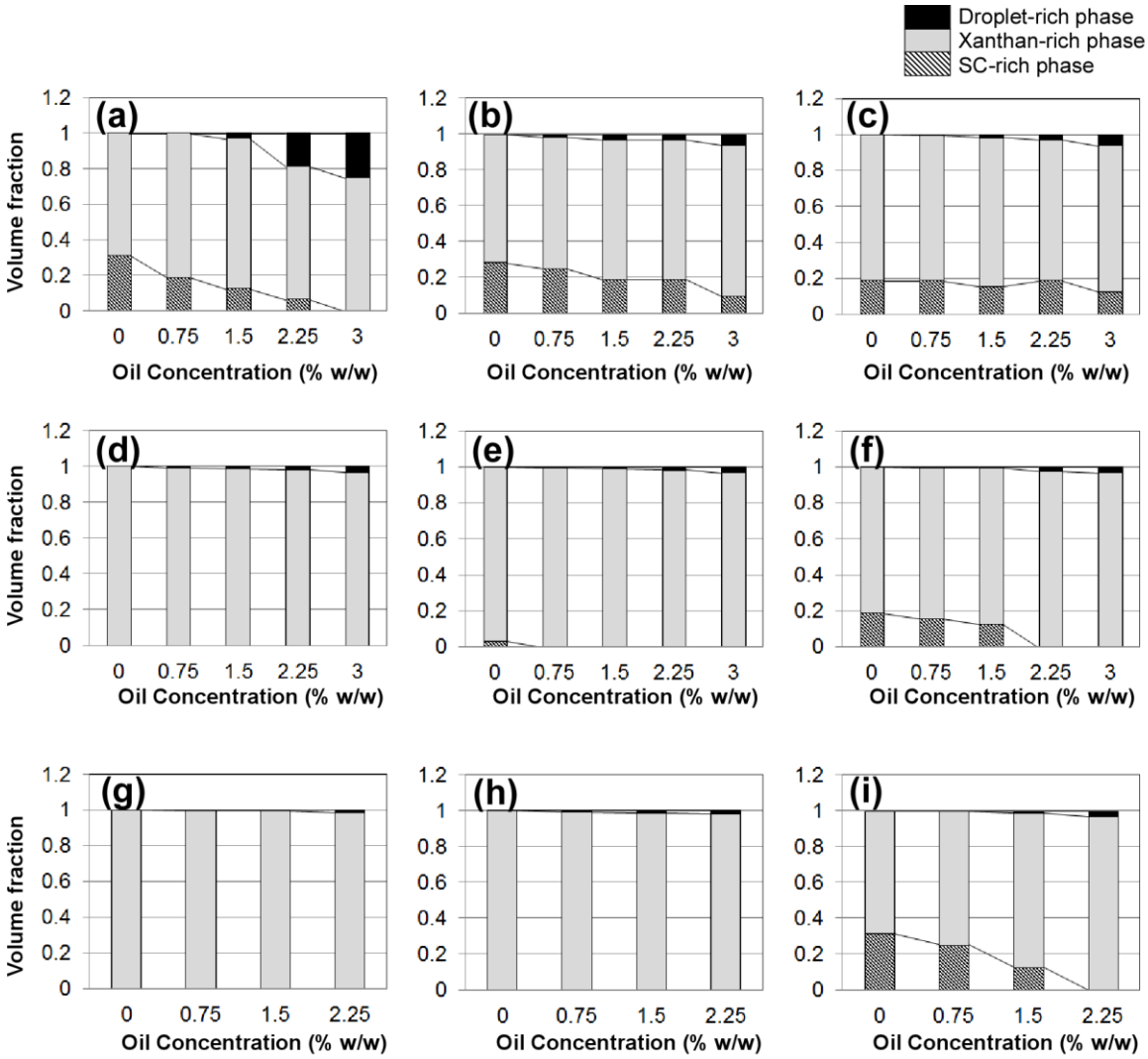

Fig. 2-4. Volume fraction of different phases of SC + xanthan mixtures at pH 6.4 at various xanthan concentrations as a function of weight % added oil droplets: 0.05% w/w xanthan (a), (d) and (g); 0.075% w/w xanthan (b), (e) and (h); 0.1% w/w xanthan (c), (f) and (i); 3% w/w SC and [Ca^{2+}] = 32 mM (a-c); 3% w/w SC and [Ca^{2+}] = 22 mM (d-f); 4% w/w SC and [Ca^{2+}] = 22 mM (g-i). Black = upper droplet-rich phase, light grey = xanthan-rich phase; hatched = lower SC-rich phase.

2.3.3. CLSM images of the mixtures

Fig. 2-5 shows CLSM images of mixtures of 4% w/w SC + 0.1% w/w xanthan 30 min after their preparation in the presence of different [Ca^{2+}] with and without 2.25 % w/w emulsion droplets. The left hand set of images, i.e., (a), (c) and (e), corresponds to the absence of droplets: the right hand set of images, i.e., (b), (d) and (f), corresponds to systems in the presence of the droplets; [Ca^{2+}] = 10 mM for the systems shown in (a) and (b), 22 mM for the systems shown in (c) and (d) and 32 mM for the systems shown in (e) and (f). Both Nile Blue and Nile Red stains were included and the fluorescent intensities in the images have been colour coded so that more blue areas correspond to more protein-rich regions, whilst more red areas correspond to more oil-rich regions. Consequently, purple areas correspond to regions where both protein and oil droplets are concentrated in close proximity. Fig. 2-5(a) clearly shows that at [Ca^{2+}] = 10 mM the microstructure is uniform, i.e., no phase separation. On the addition of droplets to this system (Fig. 2-5(b)) the background microstructure remains the same whilst some large oil droplets (or droplet aggregates) are visible. The average diameter of these oil-rich regions determined by image analysis is 5 μm, which is considerably larger than the initial droplet size (0.36 μm) determined by the Mastersizer.

At the higher [Ca^{2+}] = 22 mM, the SC + xanthan mixture clearly shows phase separation in the absence of droplets (Fig. 2-5 (c)), with protein rich regions of longest dimension10–20 μm clearly distinguishable, whilst on addition of droplets (Fig. 2-5(d)) this feature of the microstructure largely disappears but even larger oil-rich regions appear. The images therefore confirm the suppression of phase separation by addition of the droplets, but enhanced droplet flocculation also appears to take place, which explains the appearance of the third upper droplet-rich phase in the visual test tube observations (Figs. 2-3 and 2-4), since such flocs will cream more rapidly. Fig. 2-5(d) in fact shows some small, light blue regions that may be regions of incipient phase separation, which possibly sink to form the lower protein-rich phase observed in the test

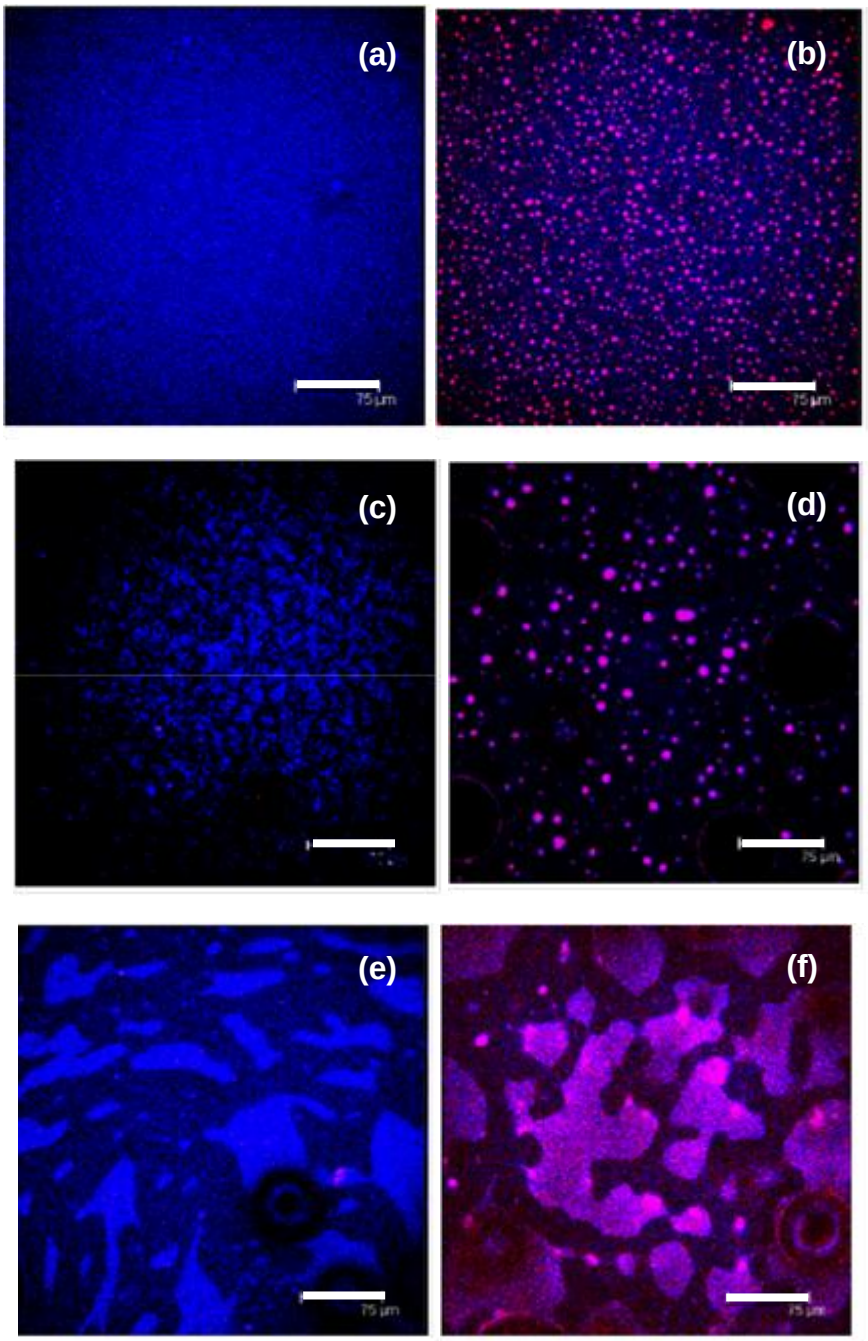

Fig. 2-5. CLSM micrographs of mixtures of 4% w/w SC + 0.1% w/w xanthan at pH 6.4, 30 min after preparation: Without 2.25% w/w oil droplets (a), (c) and (e); with 2.25% w/w oil droplets (b), (d) and (f); [Ca^{2+}] = 10 mM (a) and (b); [Ca^{2+}] = 22 mM (c) and (d); [Ca^{2+}] = 32 mM (e) and (f). Blue colour = protein-rich; red colour = oil-rich. Size bar = 75 μm.

tubes. There are also some very large circular black regions of diameter >50 μm, which I believe are air bubbles rather than pure xanthan-rich blobs, although this is difficult to confirm absolutely. Finally, Fig. 2-5(e) and (f) illustrate the microstructures observable with and without droplets, respectively, at the higher [Ca^{2+}] = 32 mM. The microstructures are very similar, with much larger protein-rich regions than at lower [Ca^{2+}]. When the droplets are present the majority of oil-rich regions appear to be located within the protein-rich regions, as previously observed by Moschakis et al. (2005, 2006) for SC-stabilized emulsions + xanthan at much higher % oil. Thus, the addition of droplets cannot apparently inhibit phase separation at the higher [Ca^{2+}], again in agreement with the discussion of the macroscopic observations in Figs. 2-3 and 2-4.

Fig. 2-6 shows the microstructure of 4% w/w SC alone (i.e., no xanthan) + the same concentration of droplets (2.25 % w/w) and [Ca^{2+}] as in Fig. 2-5(b), for comparison. Without xanthan, the oil-rich regions are clearly considerably smaller than in its presence. The objects were too small to be reliably sized by image analysis, but they were certainly less than 0.5 μm, closer to the initial droplet size of 0.36μm.

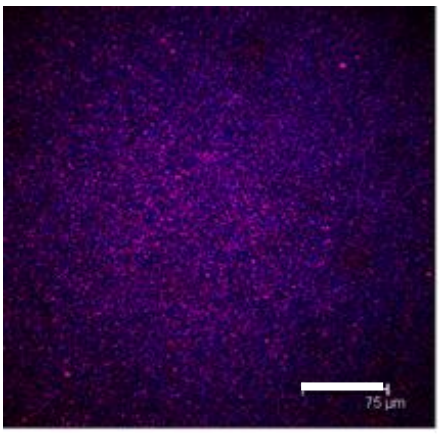

Fig. 2-6. CLSM micrographs of mixtures of 4% w/w SC at pH 6.4, [Ca^{2+}] = 10 mM, in the absence of xanthan: 30 min after preparation. Blue colour = protein-rich; red colour = oil-rich. Size bar = 75 μm.

Consequently, the larger apparent droplet sizes in the presence of xanthan are most likely due to flocs of droplets, possibly due to depletion flocculation (Flocs will tend to rise more rapidly to the top of the sample and be more predominant in the micrographs).

Fig. 2-7 illustrates the typical evolution of the microstructure with time, for 4% w/w SC + 0.1% w/w xanthan at pH 6.4 and $[Ca^{2+}]$ = 32 mM. Again, the left hand set of images, i.e., (a), (c) and (e), correspond to the absence of droplets; the right hand set of images, i.e., (b), (d) and (f), correspond to systems in the presence of 2.25% w/w emulsion droplets: images (a) and (b) were obtained 10 min after mixing; (c) and (d) 15 min after mixing, (e) and (f) 25 min after mixing. Although the droplets do not inhibit significant phase separation from taking place in under 30 min, as noted above, it is seen that the morphology of the phase separation with droplets is somewhat different. In the absence of droplets the morphology of the protein-rich regions seems more rounded and regular. This qualitative difference has been analyzed in a slightly more quantitative way using image analysis, where the roundness parameter R (= $4\pi \times$ area/perimeter^2) has been extracted for images at different times for all objects of area >67 μm^2. This arbitrary cut-off value was used to prevent background fuzziness in the images from generating large numbers of spurious small objects. Fig. 2-8 shows R versus time and it is seen that with no droplets there is a definite increase in R to more circular (R = 1) objects, whilst in the presence of droplets R persists between 0.1 and 0.2, perhaps slightly decreasing with time. This may indicate a more stiff interface between the 2 phases in the presence of the droplets.

Although the micrographs here and measurements elsewhere (Moschakis et al., 2005, 2006) suggest segregative phase separation, Kobori, Matsumoto, and Sugiyama (2009) have reached different conclusions based on analysis of the structure of SC + xanthan complexes by atomic force microscopy. They observed fibres forming between SC and xanthan at pH 6.6. Small features of height of approximately 5 nm were

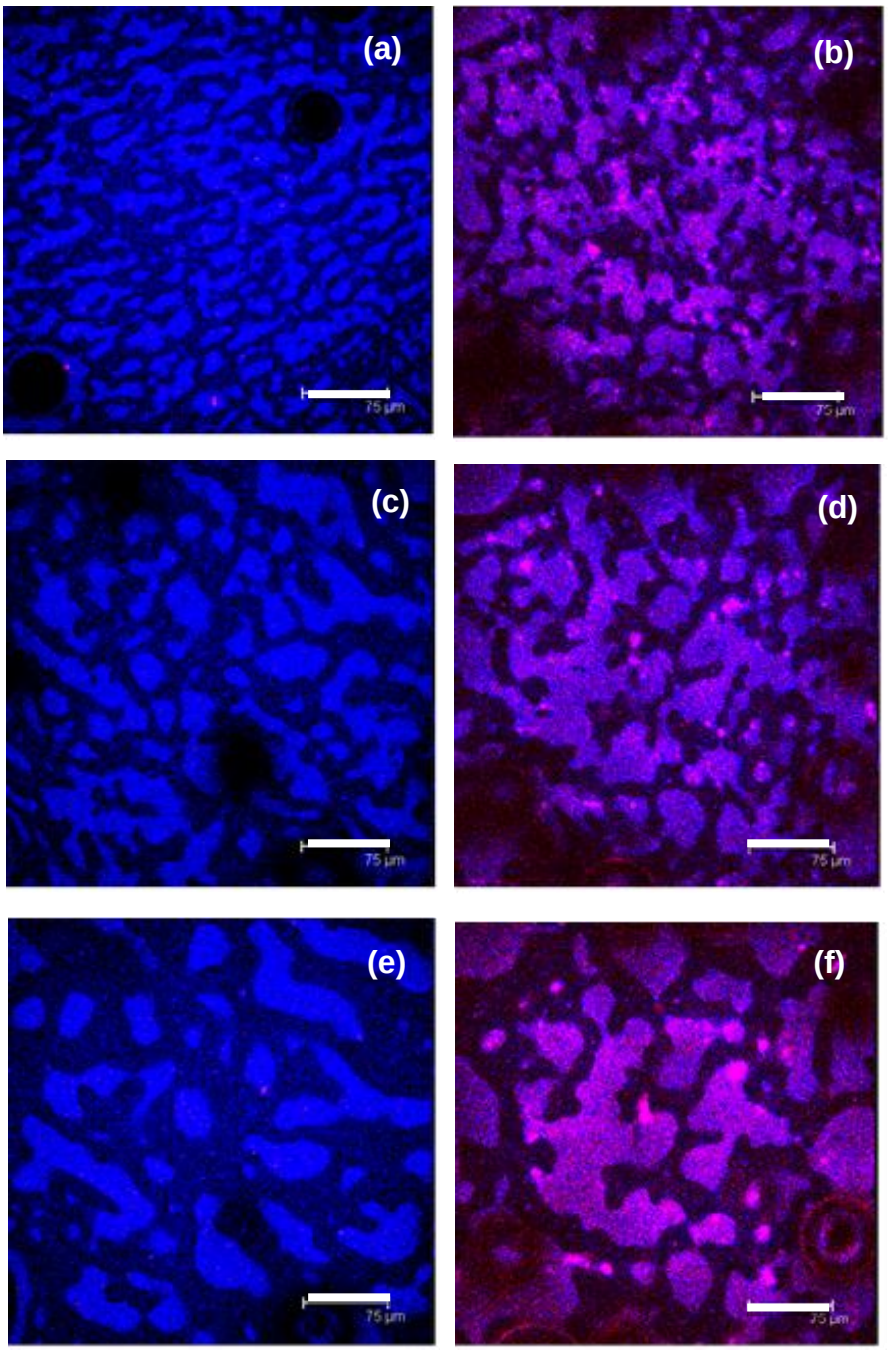

Fig. 2-7. CLSM micrographs of mixtures of 4% w/w SC + 0.1% w/w xanthan, [Ca^{2+}] = 32 mM at pH 6.4 without oil droplets (a), (c) and (e); with 2.25% w/w oil droplets (b), (d) and (f); 10 min after preparation (a) and (b); 15 min after preparation (c) and (d); 25 min after preparation (e) and (f). Size bar = 75 μm.

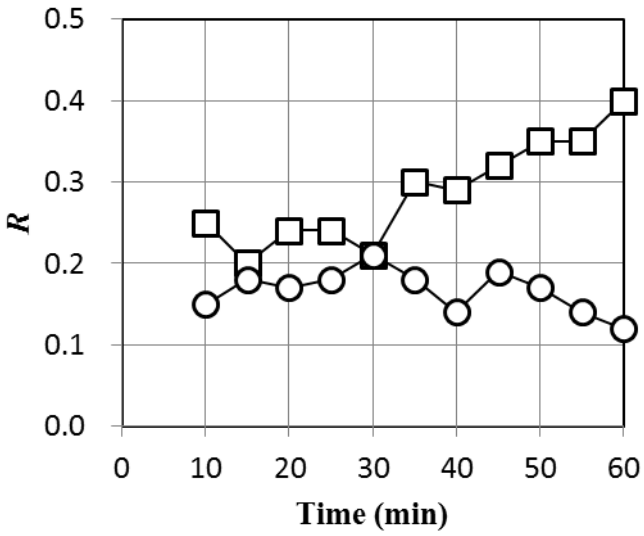

Fig. 2-8. Change in roundness parameter, *R*, versus time since mixing, obtained via image analysis of CLSM micrographs of 4 % w/w SC + 0.1 % w/w xanthan, [Ca^{2+}] = 32 mM at pH 6.4: without droplets (□); with 2.25 % w/w droplets (○).

observed on the fibrous structure, suggestive of casein sub-micelles or their fragments and it was suggested that such aggregation was the reason of loss of segregation in some SC + xanthan mixtures, i.e., where phase separation was not observed. It is possible that such aggregation is enhanced at low to moderate [Ca^{2+}], so that this was the reason why phase separation was not observed until higher [Ca^{2+}]. At higher [Ca^{2+}] and/or lower pH the increase in molecular weight of the casein aggregates will undoubtedly make the two types of biopolymer less likely to mix easily, so that it is harder for the droplets to prevent evolution of the phase separation. At the same time, higher [Ca^{2+}] and/or lower pH may also cause the droplets to aggregate, meaning that there will be a lower possible coverage of the water–water interface of the phase separating entities by droplets. On the other hand, recent work by Murray, Dickinson, and Wang (2009) has shown that lowering the pH of SC systems with a similar low volume faction of SC-stabilized *n*-tetradecane or 1-bromohexacane droplets causes a significant increase in the surface

shear viscosity of the air–water interface, so that some increase in droplet aggregation may also strengthen the interface between the SC-rich and xanthan-rich phases in the systems studied here. Particle jamming at the interface is thought be responsible for arresting phase separation in bijels. In my systems no definite preference for droplets at the outer edge of the protein-rich separating regions was observed – rather droplets seemed to be mixed in with these regions. However, this is perhaps not surprising, given that the primary droplet size is below the resolution of the CLSM under the conditions used and that the droplets were stabilized by a layer of SC, which is likely to mix into and adhere to the SC-rich phase.

2.3.4. Particle size distributions of SC

As mentioned above, one factor promoting phase separation is probably the increased aggregation of the SC as the pH is lowered and such aggregates may appear in the CLSM micrographs independent of any thermodynamically driven incompatibility between xanthan and SC. It was therefore important to try and characterize the formation of such aggregates separately, i.e., in the absence of xanthan. The particle size distribution of SC with [Ca^{2+}] was therefore measured at different pH values using the Zeta Nanosizer and Fig. 2-9 shows the results. At pH 6.4 and 5.9 the $Z_{average}$ diameter increases steadily from approximately 60 nm–200 - 300 nm as [Ca^{2+}] is increased to 40 mM, whilst at pH 5.4 the increase in size is much more dramatic, essentially off-scale (i.e., >1 μm) by [Ca^{2+}] = 10 mM. It is therefore not surprising that there is a much bigger shift in phase behaviour between pH 5.9 and 5.4 than between pH 6.4 and 5.9 (e.g., see Figs. 2-1 and 2-2). But this also means that the much larger protein-rich regions observed in the CLSM micrographs in the presence of xanthan at pH 6.4 or 5.9 were not just due to pH and calcium ion induced precipitation, but the additional effect of biopolymer incompatibility.

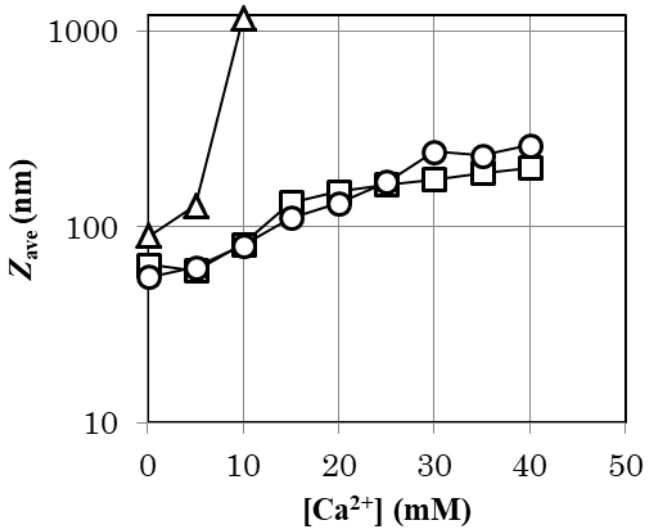

Fig. 2-9. $Z_{average}$ particle size versus [Ca^{2+}] for stock SC solutions diluted into buffers at pH: 6.4 (□); 5.9 (○); 5.4 (△).

2.3.5. Mean emulsion droplet size as function of calcium ion concentration

The CLSM micrographs showed evidence of increased droplet aggregation as [Ca^{2+}] was increased. Since the droplets appear to be confined to the protein-rich regions, the added loading of these regions with the lighter oil phase would tend to alter the gravitational separation of these protein-rich regions and above it was pointed out that the more aggregated the droplets are, the less able they will be to cover the interface between the two phases. It was therefore also important to see to what extent [Ca^{2+}] changed the particle size of the primary emulsion added. Fig. 2-10 shows d_{43} versus [Ca^{2+}] for an emulsion sample after 10 days at 20 °C at pH 6.4. Before measurement, any creamed emulsion was dispersed by gentle shaking by hand. It is seen that the average droplet size is essentially unchanged up until approximately [Ca^{2+}] = 20 mM, when significant aggregation of the droplets starts to occur, although this Ca^{2+}-induced flocculation cannot solely explain the much larger droplet aggregates observed in the CLSM micrographs in the presence of xanthan at lower [Ca^{2+}]. Such aggregates are

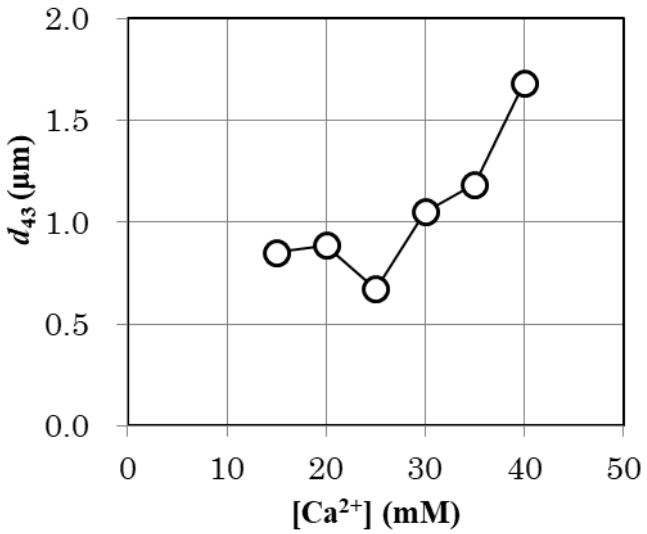

Fig. 2-10. Mean particle size (d_{43}) versus [Ca^{2+}] of stock SC-stabilized emulsion after dilution to 1 vol.% oil droplets in buffer at pH 6.4 containing the [Ca^{2+}] shown.

therefore also an additional consequence of the phase separation of the SC and xanthan and/or due to depletion flocculation of the droplets by the xanthan.

Another possible influence on the micro- and macroscopic phase separation observed is that, the protein coverage of the droplets could increase significantly as the pH or [Ca^{2+}] is changed, such that these creaming droplets carry away a significant amount of protein, lowering the local concentration of SC to levels such that the remaining [SC] + [xanthan] is in the single phase region. However, the following simple calculation show that this is very unlikely. From the surface area of the droplet size distribution at 2.25% w/w added oil droplets in a 3% w/w SC solution, for all this protein to be removed by the droplets the surface load of protein would have to be 83 mg m^{-2}. This is massively in excess of a typical surface protein load for stable emulsions, around 2 mg m^{-2} (Srinivasan, Singh, & Munro, 1999), whilst the surface load of SC-stabilized emulsions in up to 20 mM [Ca^{2+}] is still only as high as 6 mg m^{-2} according to Srinivasan, Singh, and Munro (1996). In addition, further measurements

(not shown) on a selection of systems using 1-bromohexadecane as the oil phase, which has the same density as water, gave very similar images in the CLSM, so that the density difference between the droplets and the aqueous phase is definitely not an overriding factor determining of the microstructures observed.

References

Antonov, Y. A., Lefebvre, J., & Doublier, J.-L. (1999). On the one-phase state of aqueous protein-uncharged polymer systems: casein-guar gum system. *Journal of Applied Polymer Science*, *71*, 471–482.

Araki, T., & Tanaka, H. (2006). Wetting-induced depletion interaction between particles in a phase-separating liquid mixture. *Physical Review E*, *73*, 061506.

Bourriot, S., Garnier, C., & Doublier, J.-L. (1999a). Micellar-casein-κ-carrageenan mixtures. I. Phase separation and ultrastructure. *Carbohydrate Polymers*, *40*, 145–157.

Bourriot, S., Garnier, C., & Doublier, J.-L. (1999b). Phase separation, rheology and microstructure of micellar casein-guar gum mixtures. *FoodHydrocolloids*, *13*, 43–49.

Burgaud, I., Dickinson, E., & Nelson, P. V. (1990). An improved high-pressure homogenizer for making fine emulsions on a small scale. *International Journal of Food Science & Technology*, *25*, 39–46.

Cates, M. E., & Clegg, P. S. (2008). Bijels: a new class of soft materials. *Soft Matter*, *4*, 2132–2138.

Dickinson, E. (2006). Colloid science of mixed ingredients. *Soft Matter*, *2*, 642–652.

Doublier, J.-L., Garnier, C., Renarda, D., & Sanchez, C. (2000). Protein-polysaccharide interactions. *Current Opinion in Colloid & Interface Science*, *5*, 202–214.

Firoozmand, H., Murray, B. S., & Dickinson, E. (2009). Interfacial structuring in a phase-separating mixed biopolymer solution containing colloidal particles. *Langmuir*, *25*, 1300–1305.

Hamar, Y., Tamehana, M., Munro, P. A., & Singh, H. (2001). Viscosity, microstructure and phase behavior of aqueous mixtures of commercial milk protein products and xanthan gum. *Food Hydrocolloids*, *15*, 565–574.

Kim, E., Stratford, K., Adhikari, R., & Cates, M. E. (2008). Arrest of fluid demixing by

nanoparticles: a computer simulation study. *Langmuir*, *24*, 6549–6556.

Kobori, T., Matsumoto, A., & Sugiyama, S. (2009). pH-Dependent interaction between sodium caseinate and xanthan gum. *Carbohydrate Polymers*, *75*, 719–723.

Maroziene, A., & de Kruif, C. G. (2000). Interaction of pectin and casein micelles. *Food Hydrocolloids*, *14*, 391–394.

Mimouni, A., Deeth, H. C., Whittaker, A. K., Gidley, M. J., & Bhandari, B. R. (2009). Rehydration process of milk protein concentrate powder monitored by static light scattering. *Food Hydrocolloids*, *22*, 1958–1965.

Moschakis, T., Murray, B. S., & Dickinson, E. (2005). Microstructural evolution of viscoelastic emulsions stabilized by sodium caseinate and xanthan gum. *Journal of Colloid and Interface Science*, *284*, 714–728.

Moschakis, T., Murray, B. S., & Dickinson, E. (2006). Particle tracking using confocal microscopy to probe the microrheology in a phase-separating emulsion containing nonadsorbing polysaccharide. *Langmuir*, *22*, 4710–4719.

Murray, B. S., Dickinson, E., & Wang, Y. (2009). Bubble stability in the presence of oil emulsion droplets: influence of surface shear versus dilatational rheology. *Food Hydrocolloids*, *23*, 1198–1208.

Perrechil, F. A., & Cunha, R. L. (2012). Development of multiple emulsions based on the repulsive interaction between sodium caseinate and LBG. *Food Hydrocolloids*, *26*, 126–134.

Srinivasan, M., Singh, H., & Munro, P. A. (1996). Sodium caseinate-stabilized emulsions: factors affecting coverage and composition of surface proteins. *Journal of Agricultural and Food Chemistry*, *44*, 3807–3811.

Srinivasan, M., Singh, H., & Munro, P. A. (1999). Adsorption behaviour of sodium and calcium caseinates in oil-in-water emulsions. *International Dairy Journal*, *9*, 337–341.

Stratford, K., Adhikari, R., Pagonabarraga, I., Desplat, J.-C., & Cates, M. E. (2005).

Colloidal jamming at interfaces: a route to fluid-bicontinuous gels. *Science*, *309*, 2198–2201.

Syrbe, A., Bauera,W. J., & Klostermeyer, H. (1998). Polymer science concepts in dairy systems - an overview of milk protein and food hydrocolloid interaction. *International Dairy Journal*, *8*, 179–193.

Tuinier, R., & de Kruif, C. G. (1999). Phase behaviour of casein micelles/exocellular polysaccharide mixtures: experiment and theory. *Journal of Chemical Physics*, *110*, 9296–9304.

Chapter 3

Effect of oil droplets and their soild/liquid composition on the phase separation of protein–polysaccharide mixtures

3.1. Introduction

Phase separation in biopolymer solutions has been studied for many years (Frith, 2010; Tolstoguzov, 1986). The situation is commonly encountered in aqueous food systems containing a mixture of protein (e.g., gelatin, whey protein) + polysaccharide (e.g., dextran, maltodextrin) under conditions where the protein−polysaccharide interaction is net repulsive (Butler & Heppenstall-Butler, 2003; Tromp, Rennie, & Jones, 1995). Such systems potentially provide a novel way of influencing desired texture and small molecule (flavors, drugs, etc.) release characteristics via dispersions of one type of aqueous phase in another, so-called water-in-water (W/W) emulsions. Studies (Frith, 2010; Williams et al., 2001) have shown how the detailed microstructure of W/W dispersions of protein and polysaccharide solutions can be controlled by changes in the composition and solution conditions (salt, pH, temperature, shear rate, etc.). Filaments, droplets, or bicontinuous structures can be produced. Although this is attractive, it is difficult to control because there are no obvious surfactants for W/W systems that can effectively trap the systems in the different metastable states by providing barriers to coalescence and component diffusion, and their long-term stability is reliant on gelation of one or both of the phases.

Clegg and co-workers (Clegg, & Cates, 2008; Herzig, White, Schofield, Poon, & Clegg, 2007) have recently studied the phase separation of an oil–water (lutidine–water) system in the presence of silica particles. In the absence of particles, the O–W system phase separates via spinodal decomposition. The inclusion of

increasing concentrations of hydrophobic silica particles results in a slowing down of the domain growth until at 3 vol % particle growth appears to be arrested completely (i.e., for several days) with the formation of so-called "bijels". (The term bijel refers to the apparent locking in or "jelling" of the bicontinuous oil–water structures observed). The effect was ascribed to the increasing strength of the interfacial film of particles (Clegg et al., 2007; White, Schofield, Binks, & Clegg, 2008). Such systems have also been extensively modeled by the Edinburgh group (Clegg, & Cates, 2008; Stratford, Adhikari, Pagonabarraga, Desplat, & Cates, 2005) while Laradji (2004) and Hore and Laradji (2007) have simulated filler particles reducing the growth rate of spinodal decomposition of a simple binary polymer melts. More recently Jansen and Harting (2011) have developed simulations that account for the formation of bijels in terms of microscopic fluid−particle and particle−particle interactions. However, a key feature of all of these systems is that the particles are plainly quite surface-active at the interfaces concerned; hence the effect can be explained by the accumulation of densely packed layers of particles at the interface that inhibit diffusive transport of material across the phase boundaries.

It is well-known that surface-active particles can be extremely efficient stabilizers of dispersions if the particles possess the appropriate wetting properties (i.e., contact angle) at the interface. This is because the particles can have extremely large energies of desorption (ΔG_d), of the orders of thousands of $k_B T$ per particle (Binks & Horozov, 2006).

ΔG_d is given by:

$$\Delta G_d = \gamma R^2 (1 \pm \cos\theta)^2 \qquad (3\text{-}1)$$

where γ is the interfacial tension, R is the particle radius (assumed spherical), and θ is the contact angle. Particle-stabilized systems (but largely oil/water or air/water systems) in foods have been reviewed recently by a number of authors (Dickinson, 2010, 2012, 2013; Ghosh & Rousseau, 2011; Murray, 2007). Solid (saturated) fat crystals may be an

important natural particle (Pickering) stabilizer (Gupta & Rousseau, 2012), but health concerns over saturated fat and complications controlling the fat crystal habit and size (Garti, Aserin, Tiunova, & Binyamin, 1999) mean that alternatives are probably preferable. In addition, with W/W systems the interfacial tensions can be extremely low ($\gamma \approx 0.001-0.01$ mN m^{-1}) (Wolf, Scirocco, Frith, & Morton, 2000) which at first sight might be expected to make the ΔG_d term insignificantly small. However, although γ and θ may be low, this may still translate to a non-negligible desorption energy (ΔG_d) if the particles are large enough. For example, from eq 3-1, if γ is only 0.001 mN m^{-1} and θ only 1°, if R = 100 nm, ΔG_d is still $\approx 150 k_B T$. Thus, the particles may in fact still be weakly adsorbed to one side of the interface, while Firoozmand, Murray, and Dickinson (2009) have proposed that accumulation of particles at the water–water interface of a gelatin + starch system could also be enhanced by size exclusion of the particles from either biopolymer phase. Particles of both polystyrene latex and small (<1 μm) emulsion droplets were observed to significantly change the microstructure and the dynamics of the phase separation. Balakrishnan, Nicolai, Benyahia, and Durand (2012) have recently reported accumulation of latex particles at a water–water interface for a phase-separating dextran + polyethylene oxide system. Here there was little apparent inhibition of phase separation with latex, but there was inhibition when latex was replaced with polydisperse β-lactoglobulin aggregates. The phenomenon is similar to that reported by Poortinga (2008), who created deliberately aggregating particles (polydisperse fat crystals, but also quartz, whey protein aggregates, and probiotic bacteria) at the interface between phase separating polysaccharides and proteins.

One of the hypotheses surrounding control of phase separating microstructures is that the mechanical strength of the interfacial film of particles plays a role in slowing down phase separation (Clegg & Cates, 2008; Herzig et al., 2007). Up to now, however, no direct measurements of interfacial strength appear have been made, although in principle measurement of the rate of relaxation of structures after mechanical distortion

from their equilibrium shape could be used to extract this information (Antonov, Puyvelde, & Moldenaers, 2004; Puyvelde, Antonov, & Moldenaers, 2002; Scholten, Sagis, & van der Linden, 2006; Simeone, Alfani, & Guido, 2004). Such measurements have shown that γ increases considerably the further the composition moves from the critical point where phase separation occurs, while Cheng and Velankar (2009) have used the droplet relaxation technique to specifically look at particle jamming effects in oil–water systems.

Interfacial shear rheology is particularly sensitive to the composition and interactions at an interface (Murray, 2002), as demonstrated in studies of competitive absorption between proteins and low molecular weight surfactants, plus interfacial interactions between different proteins and between proteins and polysaccharides (Krägel, Derkatch, & Miller, 2008; Dickinson, 2011). In addition, interfacial shear viscosity (η_i) has been shown to be sensitive to the accumulation of particles at interfaces in the presence of protein. For example, Murray, Dickinson, and Wang (2009) demonstrated a significant increase in η_i at the air−water interface in the presence of stable O/W emulsion droplets when sodium caseinate was also adsorbed, while even larger increases in η_i were seen in the presence of surface active cellulose particles and starch granule fragments (Murray, Durga, Yusoff, & Stoyanov, 2011). Recently Safouane, Langevin, and Binks (2007) reported extremely stiff films of partially hydrophobic particles at the air−water interface.

The question remains whether particles can be used in general to influence phase separation in biopolymer mixtures and if so what type of food-grade particles might be used. In the study by Firoozmand, Murray, and Dickinson (2009) referred to above, caseinate-stabilized emulsion droplets were shown to influence of phase separation gelatin and starch. In a more recent study (Hanazawa & Murray, 2014) this approach was extended to sodium caseinate + xanthan, where again it was shown that a relatively low fraction (up to 2.25% w/w) of small (<1 μm) *n*-tetradecane droplets could

also inhibit phase separation of the system to some extent, depending upon the calcium ion concentration ([Ca^{2+}]). To test the idea that increased strength of the interfacial particle network might enhance this inhibitory effect, in this study I have tested the effect of the solid/liquid fraction of the droplets, since partially solid droplets could undergo partial coalescence and lead to a stronger network. Behavior at [Ca^{2+}] = 22 or 32 mM was chosen based on the previous results (Hanazawa & Murray, 2014), since in this region phase separation in the absence of droplets is variable but significant and easy to measure. At lower [Ca^{2+}] it is more difficult to detect, while at higher [Ca^{2+}] high insolubility of SC makes the preparation of mixtures very difficult in the first place.

3.2. Materials and methods

3.2.1. Materials

Spray-dried sodium caseinate (82% w/w dry protein, 6% w/w moisture, 6 % w/w fat and ash) was supplied by DMV International (Veghel, Netherlands). The calcium concentration of the sodium caseinate (SC) sample was determined by atomic absorption as 0.78 mg g^{-1}. A food-grade xanthan gum powder (Keltrol, product code 0F8209A) was obtained from CP Kelco UK, Surrey, UK. Eicosane (99%) was obtained from Sigma–Aldrich, (Gillingham, UK) and *n*-tetradecane (99%) from Alfa Asear (Heysham, UK). AnalR grade sodium azide, $CaCl_2.H_2O$, imidazole, sodium hydroxide, and hydrochloric acid were also obtained from Sigma–Aldrich (Gillingham, UK), as were Nile Red and Nile Blue dyes for confocal microscopy. Water purified by treatment with a Milli-Q apparatus (Millipore, Bedford, UK) with a resistivity not less than 18.2 MΩ cm was used for the preparation of all aqueous solutions. Sodium azide was added to all aqueous solutions at 0.02% w/w as an antimicrobiological agent.

3.2.2. Mixture preparation

Stock solutions of sodium SC were prepared by dispersing 6.25% w/w protein in water by gentle stirring for 1 h. The [Ca^{2+}] in protein stock solutions was adjusted to 27.5 or 54 mM by addition of $CaCl_2 \cdot H_2O$ solution. The pH of the SC solutions was adjusted to pH 6.4 by addition of 0.1 mol dm^{-3} NaOH. In the final SC solutions, the SC concentration was 5% w/w. Stock solutions of 2% w/w xanthan were prepared by dispersing the gum in 0.02 M imidazole buffer (previously adjusted to pH 6.4 by addition of 0.1 mol dm^{-3} HCl or NaOH) with gentle stirring and kept overnight in a refrigerator before use. A 2.5% w/w SC solution was prepared in the pH 6.4 imidazole buffer as an emulsifier. Oil-in-water (O/W) emulsions were prepared with a range of compositions, from 100% *n*-tetradecane (TD) to 100% eicosane (EC), and their effects on phase separation studied. For brevity, here I only present results for pure TD, pure EC, and the mixture of 50% w/w TD + 50% w/w EC, hereafter referred to as the mixed oil system. O/W emulsions were prepared by using a jet homogenizer (Burgaud, Dickinson, & Nelson, 1990) operating at 300 ± 20 bar with 2.5% w/w SC as the aqueous phase. The oil phase, 2.5% w/w SC solution, and the jet homogenizer were heated to 60−65 °C when preparing the EC and mixed systems to ensure that the oil phase was completely liquid during emulsification. The TD emulsion was prepared at room temperature (20−25 °C). All emulsions were then stored overnight in a refrigerator before further use to ensure that any EC crystallization was complete. Allen, Murray, & Dickinson (2008b) have shown how pure EC droplets prepared in a similar way retain their spherical shape and droplet size distribution despite crystallization of the oil phase. In all the final emulsions, the SC concentration was 2% (w/v), and the concentration of dispersed oil phase was 20 vol %.

Particle size distributions of emulsions were measured via a Malvern Mastersizer Hydro 2000 (Malvern Instruments Ltd., UK). For all emulsions the refractive index of the oil was taken as 1.460 and that of the dispersion medium 1.330.

The absorbance of proteins was assumed 0.001. For all types of emulsions d_{32} = 0.4 ± 0.04 μm. Mixtures of SC + xanthan ± emulsion were prepared in 7 mL glass vials (Ø 23 mm × H 34 mm, from VWR International Ltd., UK) and mixed by an Ultra Turrax T25 homogenizer (IKA–Werke GmbH & Co., Germany) at 9500 rpm at room temperature for 3 min. The [Ca^{2+}] was adjusted by addition of $CaCl_2 \cdot H_2O$. Any bubbles that formed during mixing were destroyed by brief bursts of ultrasound from an ultrasonic probe (Vibra-Cell VC 130, Sonics & Materials, Inc., Newtown, USA). This was to ensure that, as far as possible, bubbles did not obscure the boundaries of the different phases that formed subsequently, or become trapped within these phases.

3.2.3. Determination of phase separation.

The SC + xanthan ± droplet mixtures were kept for 24 h at room temperature and phase separation was observed visually. SC-rich phase volume fractions were calculated by dividing the height of the (lower) SC-rich phase by the total height of the mixture.

3.2.4. Confocal microscopy.

A Leica TCS SP2 confocal laser scanning microscope (CLSM) was used, mounted on a Leica Model DM REX microscope base. A 40× oil-immersion objective with numerical aperture 1.25 used, with the CLSM was operated in fluorescence mode. A staining solution of 0.01% (w/v) Nile Red in 1,2-propanediol was used to stain the oil phase and 0.01% (w/v) of Nile Blue in Milli-Q water to stain the protein. The staining solutions were stored in the dark when not in use. Fluorescence from Nile Red was excited with the 488 nm laser line, fluorescence from Nile Blue by the 633 nm laser line. Five minutes after preparation of the SC + xanthan ± emulsion mixtures, samples of approximately 3 mL were transferred to a small vessel and mixed with 30 μL of the Nile Red and/or Nile Blue dye solutions by shaking by hand. The sample was then

immediately placed into a welled slide 30 mm diameter and 0.3 mm in depth. A coverslip (0.17 mm thickness) was placed on top of the well. Micrographs started to be recorded 30 μm below the coverslip approximately 10 min after the mixture preparation. The concentrations of dyes, laser intensity, laser exposure time, and so forth, were optimized as far as possible to enable simultaneous visualization of oil-rich and protein-rich regions, although the primary droplet size (0.4 μm) was too small to be resolved with this microscope setup. Image analysis was performed using Image-Pro Plus software.

3.2.5. Interfacial shear viscosity.

The apparent interfacial shear viscosity (η_i) was measured using a two-dimensional Couette-type interfacial viscometer described many times previously (Murray, Dickinson, & Wang, 2009). A stainless steel biconical disk (radius 14.7 mm) was suspended from a thin torsion wire with its edge in the plane of the interface. The sample was located in a glass dish (radius 72.5 mm). Torsion wires of appropriate thickness and length were chosen to give a torsion constant in the required range. The motion of the disk was monitored via a 1 mW laser beam reflected onto a diode array from a mirror fixed to the spindle of the disk. The viscometer was operated in fixed shear rate mode, where the dish was rotated at constant angular velocity, $\omega = 0.635 \times 10^{-3}$ rad·s^{-1}. The disk rotates until the stress at the interface is balanced by the corresponding torque in the torsion wire. The constant shear-rate apparent interfacial viscosity, η_i, is given by:

$$\eta_i = (\theta_i - \theta_0) K \frac{g_f}{\omega} \qquad (3\text{-}2)$$

where K is the torsion constant of the wire, θ_i is the equilibrium deflection of the disc in the presence of the interfacial film, and θ_0 is the equilibrium deflection of the disc in the absence of the film, due to bulk phase drag on the upper and/or lower surface of the disk. The geometric factor, g_f, is given by

$$g_f = \frac{1}{4\pi}\left(\frac{1}{a^2} - \frac{1}{b^2}\right) \quad (3\text{-}3)$$

where *a* and *b* are the radii of the dish and the disk, respectively.

In these measurements the height of the disk had to be set so that the disk was positioned at the interface that would form between the protein-rich and xanthan-rich phases. This was achieved by making up larger volumes (300 mL) of the SC + xanthan ± emulsion. An OST 20 overhead stirrer (IKA–Werke GmbH & Co., Germany) at dial setting 7 was used with a propeller stirrer R 1342 (IKA–Werke GmbH & Co., Germany) to mix the system for 3 min. The mixture was then kept at room temperature for 24 h in order for two macroscopic phases to form. The lower (SC-rich) phase was gently removed with a pipet and added to the rheometer dish until its height was touching and level with the edge of the disk. A set volume of the upper (xanthan-rich) phase was then gently layered on top of the lower phase in the dish. The system was then left for a further 24 h for the system to re-establish a coherent interface. Since the two phases had already been pre-equilibrated, it was assumed that any slight change in the height of the interface between the two phase, due to changes in their relative volumes, would be negligible. Hence, as far as a true macroscopic interface existed, the plane of the disk edge was positioned as close as possible to this interface. The contribution due to the bulk drag of each phase on the disk was determined simply by altering the height of the disk so that it was 1 cm above or below this interfacial region, that is, completely submerged in either single phase and measuring the deflection under shear. The value of θ_0 was taken as the highest value for the disk submerged in either phase. Between individual measurements on different systems the dish of the interfacial rheometer was cleaned with ethanol and hexane and rinsed with copious amounts of pure water. The disc was cleaned by rinsing with pure water and acetone and flash-heating in a blue Bunsen flame.

3.3. Results and discussion

3.3.1. Effect of oil droplet composition on phase separation.

Fig. 3-1 shows the effect of the addition of up to 2.5% w/w TD emulsion to the system containing 4% w/w SC + 0.1% w/w xanthan, at pH 6.4 and [Ca^{2+}] = 22 or 32 mM. The results are presented in terms of the ratio of the volume fraction (ϕ) of the SC-rich phase in the presence of the droplets to the volume fraction (ϕ_0) of the SC-rich phase fraction of the mixture in the absence of the droplets. Thus, the lower the value of ϕ/ϕ_0, the greater is the inhibition of phase separation. (The absolute values of ϕ_0 were 0.35 and 0.42 at [Ca^{2+}] = 22 mM and 32 mM, respectively, and the full phase diagram of SC + xanthan at pH 6.4 is given in Fig. 2-1(a).) It seen that there is significant inhibition of phase separation only at [Ca^{2+}] = 22 mM. At [Ca^{2+}] = 32 mM the driving force for phase separation is too strong for TD droplets to exert an influence: these effects were described previously (Hanazawa & Murray, 2014). In this previous work it was explained how the creaming and sedimentation of the microscopically evolving SC- and xanthan-rich regions, leading to macroscopic phase separated layers, depended on

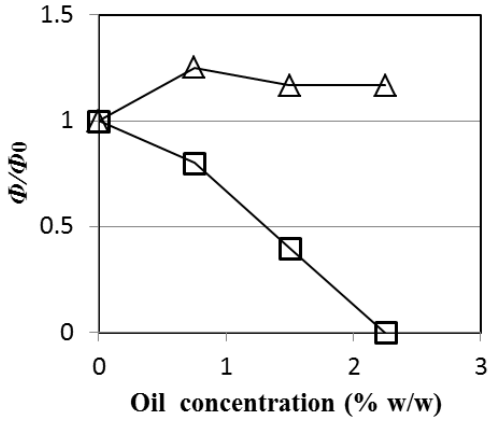

Fig. 3-1. Ratio (ϕ/ϕ_0) of the volume of the SC-rich phase separating with: without different weight % of *n*-tetradecane emulsion droplets in 4% w/w sodium caseinate + 0.1% w/w xanthan and 22 mM [Ca^{2+}] (□) or 32 mM [Ca^{2+}] (∆).

the relative concentrations of SC, xanthan, and Ca^{2+}. Increasing added Ca^{2+} from 0 to 40 mM enhances the phase separation by changing the molecular weight of the casein micelle aggregates. Sometimes a third, low volume droplet-rich phase appears on top of the macroscopic SC-rich layer, while any aggregation between the droplets and the microscopic SC-rich regions tends to increase the speed of separation of the upper SC-rich layer from the lower xanthan-rich layer. However, in this paper we wish to focus on the effect of the solid/liquid ratio of the droplets.

Fig. 3-2(a) shows the same data as Fig. 3-1 at $[Ca^{2+}]$ = 22 mM, but also for when the oil phase was the mixed system and 100% w/w EC, while Fig. 3-2(b) is the corresponding plot at the lower SC concentration of 3% w/w. It is seen in both cases that a lower concentration of droplets is required to reduce ϕ/ϕ_0 to zero (i.e., complete inhibition of phase separation) for the mixed oil system, while the 100% w/w EC droplets are the least effective. Indeed, at SC = 4% w/w (Fig. 3-2(a)), ϕ/ϕ_0 is seen to increase back toward $\phi/\phi_0 = 1$ above oil concentration = 0.75% w/w. Figs. 3-2(c) and (d) show the same type of plot and for the same conditions as in parts (a) and (b), but at the higher $[Ca^{2+}]$ = 32 mM. Overall, ϕ/ϕ_0 is again lowest for the mixed oil system, but as noted above, at higher $[Ca^{2+}]$ the emulsion droplets are less effective at inhibiting phase separation and in fact phase separation seems to be considerably enhanced by the droplets at the higher SC concentration of 4% w/w (Fig. 3-2(c)), particularly for the 100% w/w TD droplets.

The switch to promotion of phase separation by droplets under conditions where the driving force for phase separation is stronger, that is, at combinations of higher concentrations of SC and/or $[Ca^{2+}]$, was noted previously (Hanazawa & Murray, 2014), where it was also shown that this was accompanied by more extensive aggregation of the SC-coated droplets by the calcium ions. (The driving force is stronger because of the increase in size, or effective molecular weight, of the casein

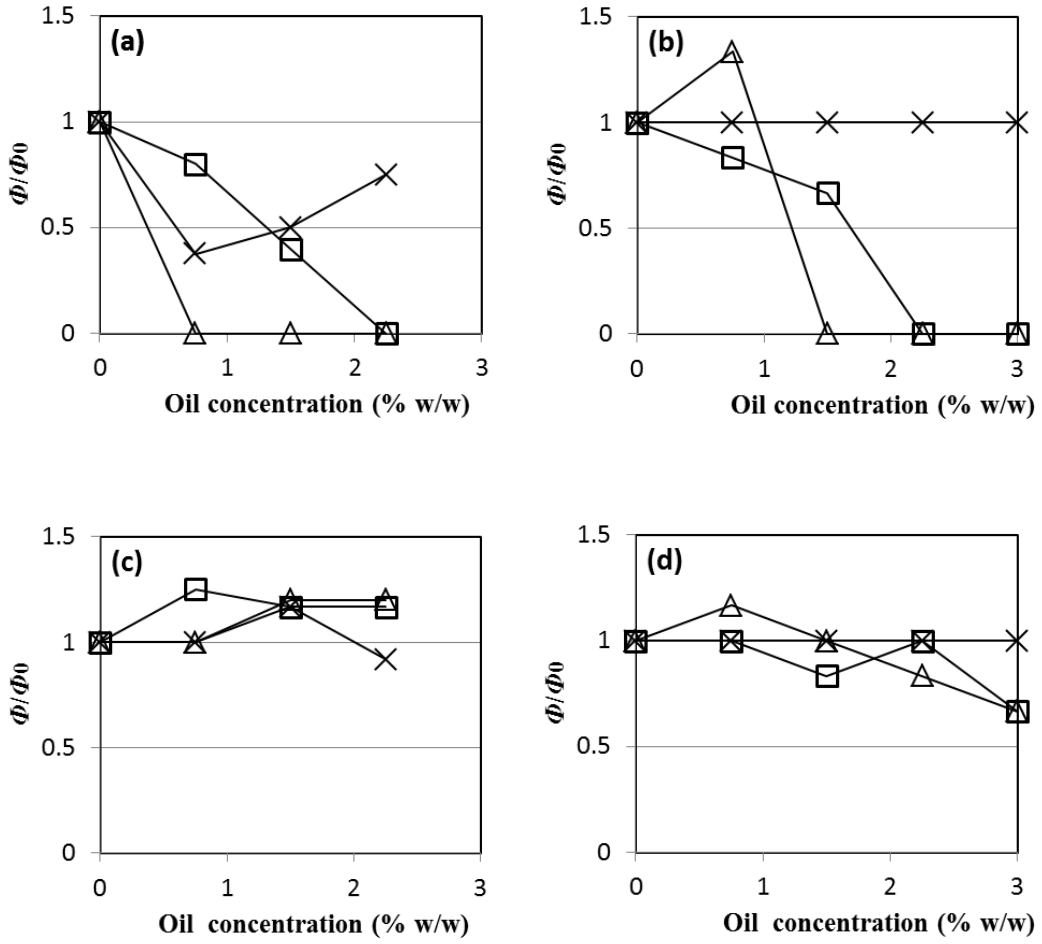

Fig. 3-2. Ratio (ϕ/ϕ_0) of the volume of the SC-rich phase separating with: without different weight % emulsion droplets of different composition: *n*-tetradecane (□); 50:50 mixture of *n*-tetradecane and eicosane (△); eicosane (×). Results are shown for 0.1% w/w xanthan and: [Ca^{2+}] = 22 mM for (a) 4% w/w SC; (b) 3% w/w SC; also [Ca^{2+}] =32 mM for (c) 4% w/w SC; (d) 3% w/w SC.

micelles as [Ca^{2+}] increases (Hanazawa & Murray, 2014), that increases their distinction from the random coil xanthan molecules.) Depletion flocculation of droplets by the relatively high concentrations of protein and xanthan probably occurs and contributes to some of the large droplet aggregates formed, plus the formation of a thin

separate-oil-rich region at the top, as noted above. Unfortunately this also means that there is no easy way of knowing the oil-to-protein ratio in the caseinate-rich regions (although it is likely to be low) and whether or not this might affect the microviscosity and structuring of these regions.

3.3.2. Effect of oil droplet composition on the microstructure of the phase-separating structures.

Fig. 3-3 shows representative CLSM images of mixtures of 4% w/w SC + 0.1% w/w xanthan + 22 mM [Ca^{2+}] ± 2.25% w/w oil droplets of varying composition, 20 min after their preparation. The circular pink regions correspond to strong Nile Red fluorescence, that is, oil droplets or their aggregates; the background blue regions correspond to strong Nile Blue fluorescence, that is, protein. Dark areas in the micrographs, that is, nonfluorescent regions, depleted of both Nile Red and Nile Blue, are assumed to be the xanthan-rich regions. Occasionally a much larger circular object surrounded by a thin fringe of Nile Red fluorescence (oil droplets) was seen in the micrographs–such features were air bubbles, which were difficult to remove completely in some instances. Examples of all four types of regions are indicated in Fig. 3-3. Samples for CLSM were taken early on in the history of mixtures before any macroscopic phase separation was apparent, because obviously it was not possible to reproducibly take samples from specific heights, plus removing a sample itself involved gentle mixing stirring the mixture. However, once the samples were in the welled slides for CLSM, within the small sample height (0.3 mm) there was minimal stratification of the material, that is, rising of protein-rich domains and/or sinking of xanthan rich domains, in the time it took to obtain the images. (Occasional large bubbles or oil droplets observed did stratify much more quickly of course.) Only if the slides were left for the same time-scales as for the macroscopic observations (i.e., 24 h) was significant variation in domain number and size observed at different heights in the microscopic

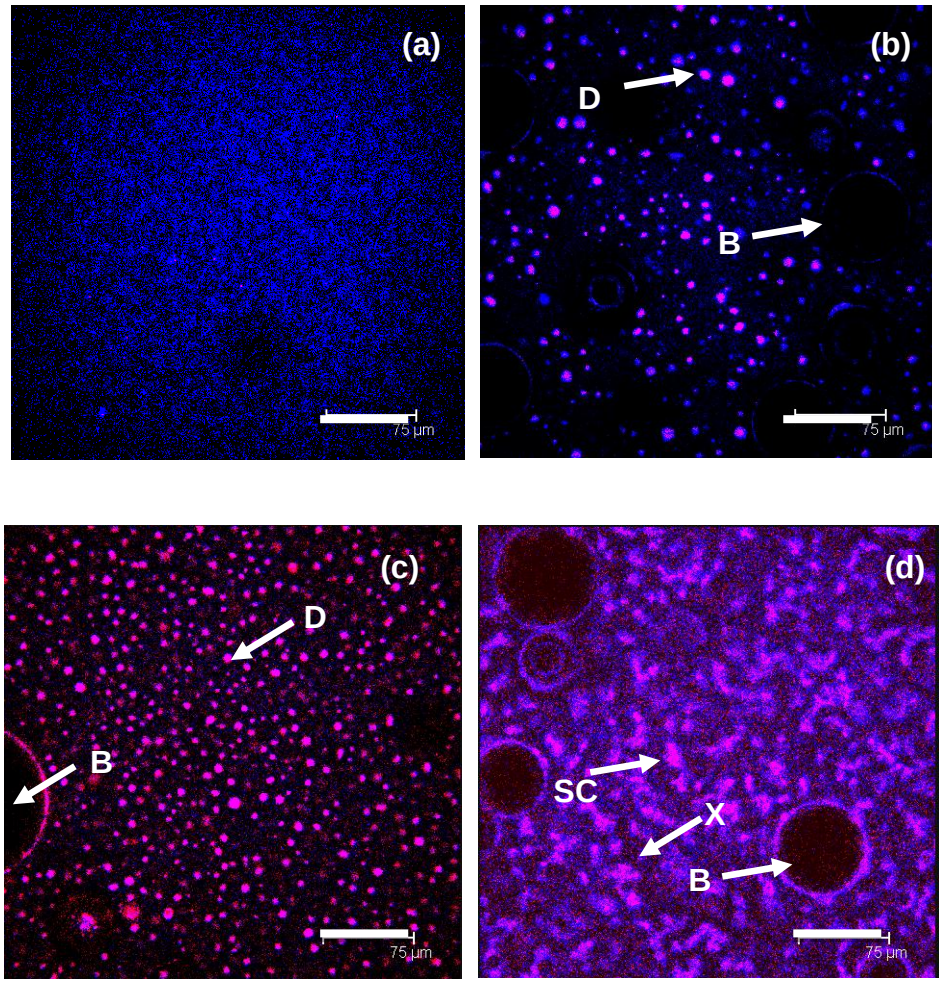

Fig. 3-3. The 20-min-old microstructures of mixtures of 4% w/w SC + 0.1% w/w xanthan + [Ca^{2+}] = 22 mM ± 2.25% w/w emulsion droplets of different composition: (a) without droplets; (b) *n*-tetradecane; (c) 50:50 mixture of *n*-tetradecane and eicosane; (d) eicosane. The arrows and labels indicate examples of air bubbles (B); droplets or droplet aggregates (D); SC-rich regions (SC); xanthan-rich regions (X). Size bar = 75 µm.

samples. The CLSM images therefore capture the phase separating structures that form early on but that eventually lead to the macroscopic phase separation observed.

Fig. 3-3(a) represents the microstructure typically observed with no added

droplets. The system is not quite uniform–protein-rich regions and xanthan-rich regions of longest dimensions 10−20 μm are distributed throughout, indicating a microstructure typical of the early onset of phase separation via spinodal decomposition. However, Fig. 3-3(b) illustrates that, when TD droplets are present, the phase-separating microstructure seen in Fig. 3-3(a) is absent. However, some oil-rich (pink) spots start to appear, of typical diameter 10 μm. Although these regions appear to be fairly circular, 10 μm is much larger than the primary emulsion droplet size (0.4 μm), so that these features must be aggregates of droplets. Fig. 3-3(c) shows a typical image of the system where the oil droplets are composed of the mixed oil system (50% w/w TD + 50% w/w EC). The microstructure is similar to that of Fig. 3-3(b), although the oil-rich regions are more numerous and prominent. Fig. 3-3 therefore seem to confirm the macroscopic observations summarized in Figs. 3-2(a) and (b), that droplets of TD and the mixed oil suppress phase separation. In contrast, Fig. 3-3(d) confirms that the EC droplets do not inhibit phase separation, rather that they seem to enhance it, as indicated by the appearance of the larger amorphous purple and black regions. These are presumed to be concentrated regions of droplets + SC and xanthan, respectively.

Fig. 3-4 quantifies the differences between images obtained for the different systems described above. Image analysis was used to measure the mean area (A_m), coefficient of variation of the area (CV), and roundness parameter ($R = 4\pi \times$ area/perimeter^2) of the SC-rich phase separating regions versus time. The number of objects analyzed for each data point was in all cases >50, but regions with apparent A_m < 6 μm^2 were excluded from the analysis because such regions were difficult to distinguish from the background "noise" in the images. In Fig. 3-4(a), it is seen that without droplets $A_m \approx 70$ μm^2 after 10 min and increases to approximately 115 μm^2 after 40 min but thereafter decreases to around 95 μm^2 in the following 20 min. The rise in A_m obviously reflects the growth of the phase separating SC-rich regions with time discussed above, while the slight decrease in A_m at longer times is a reflection that the

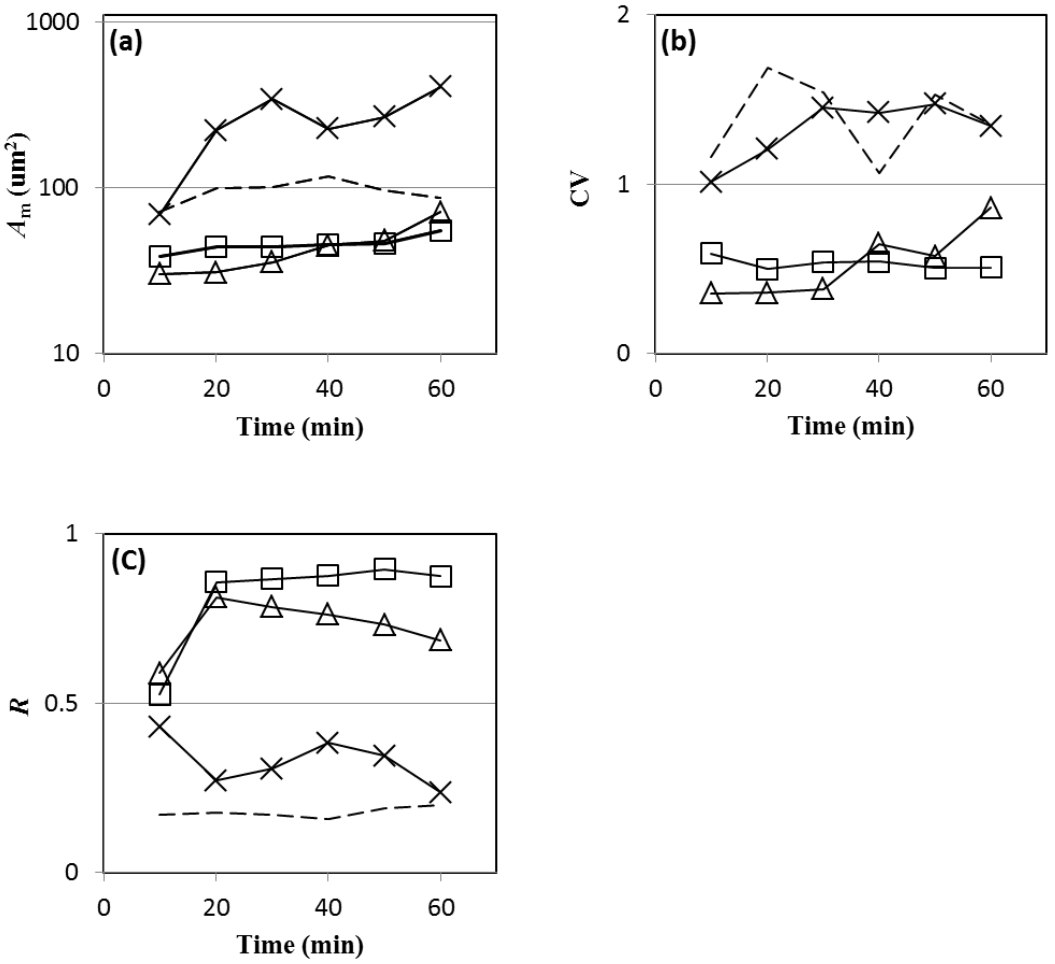

Fig. 3-4. Variation as a function of time of characteristic parameters of the microstructure: (a) mean area (A_m); (b) coefficient of variation of area (CV); (c) roundness (R): for 4% w/w SC + 0.1% w/w xanthan + [Ca^{2+}] = 22 mM ± 2.25% w/w emulsion droplets of different composition: *n*-tetradecane (□); 50:50 mixture of *n*-tetradecane and eicosane (△); eicosane (×). The dashed lines indicate the trends without droplets.

larger these regions become, the faster they tend to sink out of the field of view to form a lower bulk SC-rich phase. It is also seen in Fig. 3-4(a) that A_m is substantially reduced in the presence of either TD or the TD+EC droplets, increasing from approximately 35 μm^2 to 65 μm^2 between 10 min to 60 min after preparation. In contrast, in the presence

of pure EC droplets, A_m were substantially larger, increasing to approximately 300 μm^2.

Fig. 3-4(b) shows the coefficient of variation (CV) of the area of these separating regions and confirms the stabilizing effect of the TD and mixed oil droplets, since CV is substantially lower (0.5 ± 0.2) for the TD or mixed droplets compared to CV = 1.3 ±0.3 for the EC droplets. The roundness parameter (*R*) extracted (Fig. 3-4(c)) is lowest but most stable for the system without droplets and highest with the TD and mixed oil droplets. (Note *R* increases to a value of 1 as the shape becomes closer to a perfect circle). The *R* values with the pure (solid) EC droplets are higher but closer to those of the system without droplets. These differences in *R* values are more difficult to interpret: low values may indicate a lower tension interface more liable to random perturbations due to Brownian motion and convection but may also mean a more rigid interface that takes more time to relax back to its equilibrium curvature after such perturbations. On the other hand, the lower values of *R* may also be a reflection of the variation of sizes of structures in the absence of the droplets. Nevertheless, this component of the image analysis confirms that the droplets can have a significant effect on the phase-separating microstructure.

Fig. 3-5 shows a similar set of micrographs as Fig. 3-3 for 4% w/w SC + 0.1% w/w xanthan after 20 min, but in this case the images are representative of those observed at the higher $[Ca^{2+}]$ = 32 mM, in the presence (a) no droplets, (b) 2.25% w/w TD droplets, (c) 2.25% w/w mixed oil droplets, and (d) 2.25% w/w EC droplets. It is obvious comparing Figs. 3-3 and 3-5 that more extensive phase separation occurs in all of these systems at the higher $[Ca^{2+}]$, as noted earlier (Fig. 3-1). Fig. 3-6 confirms this further, via analyzing the images in the same way as in Fig. 3-4. Thus Fig. 3-6(a) shows A_m versus time, and for all of the systems A_m values are considerably larger than at $[Ca^{2+}]$ = 22 mM (Fig. 3-4(a)). The only exception is the system in the presence of pure EC (solid) droplets at longer (>30 min) times, where A_m is apparently lower at $[Ca^{2+}]$ = 32 mM, but again this may be an artifact of accelerated settling out of the SC-rich

regions. A_m is also seen to decrease with time after 20 min in the absence of droplets at $[Ca^{2+}]$ = 32 mM, probably for the same reasons. In contrast, in the presence or absence of the TD or mixed (TD + EC) droplets, A_m is 10−100 times larger at $[Ca^{2+}]$ = 32 mM compared to $[Ca^{2+}]$ = 22 mM such that the order of magnitude of A_m is completely reversed, that is, A_m decreases in size in the order TD droplets > TD + EC droplets > no droplets > EC droplets at $[Ca^{2+}]$ = 32 mM.

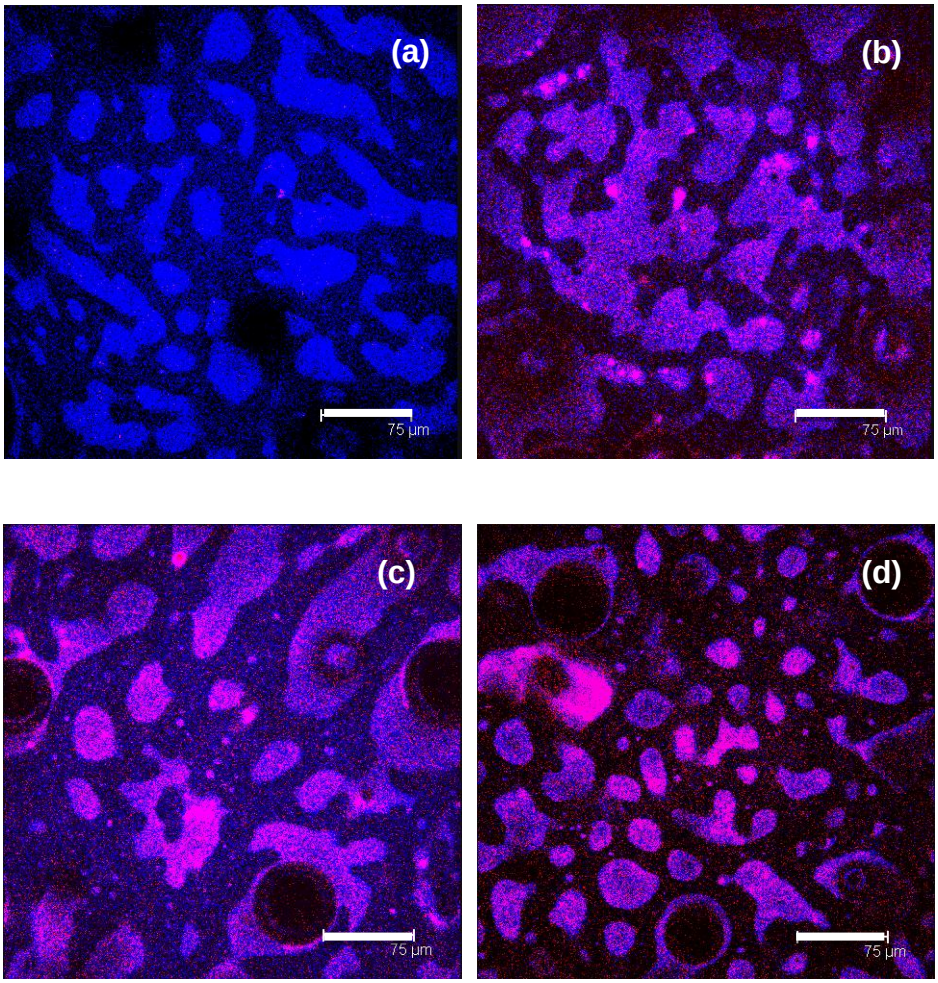

Fig. 3-5. The 20-min-old microstructures of mixtures of 4% w/w SC + 0.1% w/w xanthan + $[Ca^{2+}]$ = 32 mM ± 2.25% w/w emulsion droplets of different composition: (a) without droplets; (b) *n*-tetradecane; (c) 50:50 mixture of *n*-tetradecane and eicosane; (d) eicosane. Size bar = 75 µm.

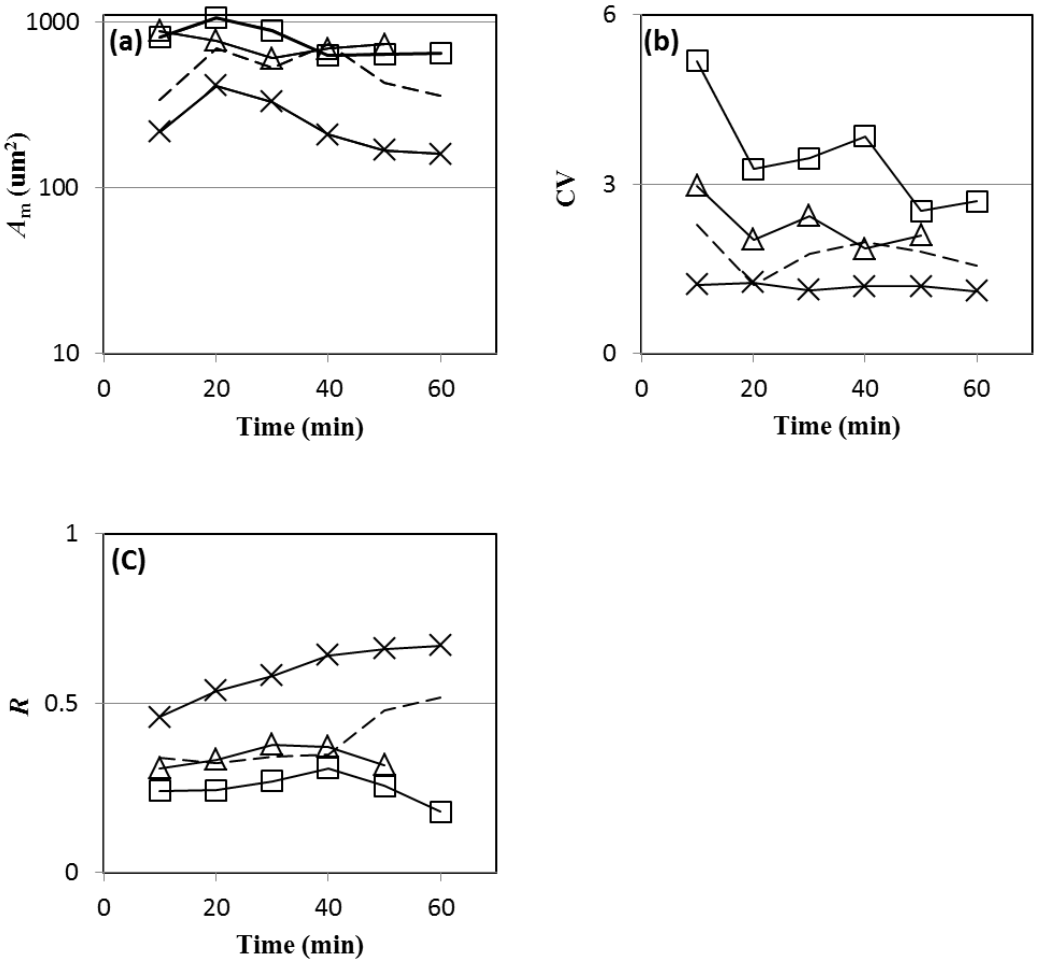

Fig. 3-6. Variation as a function of time of characteristic parameters of the microstructure: (a) mean area (A_m); (b) coefficient of variation of area (CV); (c) roundness (R): for 4% w/w SC + 0.1% w/w xanthan + [Ca^{2+}] = 32 mM ± 2.25% w/w emulsion droplets of different composition: *n*-tetradecane (□); 50:50 mixture of *n*-tetradecane and eicosane (△); eicosane (×). The dashed lines indicate the trends without droplets.

The coefficient of variation (CV) of A_m at [Ca^{2+}] = 32 mM is shown in Fig. 3-6(b). A comparison of Fig. 3-6(b) with Fig. 3-4(b) ([Ca^{2+}] = 22 mM) shows that there is hardly any difference in CV for the systems with or without EC droplets, whereas CV is significantly higher at [Ca^{2+}] = 32 mM than [Ca^{2+}] = 22 mM for the systems with

TD or TD + EC droplets and particularly the latter. At [Ca^{2+}] = 22 mM CV was lowest for the mixed droplet system. Finally, Fig. 3-6(c) shows the *R* parameter at [Ca^{2+}] = 32 mM for the different droplet systems, and a comparison with the same analysis at [Ca^{2+}] = 22 mM (in Fig. 3-4(c)) again shows a reversal in the order of magnitude of the shape analysis parameter: *R* increases in the order TD droplets > TD + EC droplets ≈ no droplets > EC droplets at [Ca^{2+}] = 32 mM, while the order is the opposite at [Ca^{2+}] = 22 mM.

In summary, it is seen that at the lower [Ca^{2+}] the TD and particularly the mixed TD + EC droplets appear to slow down phase separation, while at the higher [Ca^{2+}], they appear to give rise to a larger mean size and wider variation in size of the phase separated regions at the same aging time, that is, the promotion of phase separation. In previous studies (Hanazawa & Murray, 2014; Moschakis, Murray, & Dickinson, 2005, 2006), it has been noted how when oil droplets are present in phase separating SC + xanthan systems the majority of oil-rich regions appear to be located within the SC-rich regions, which is natural enough, since the droplets are coated by a stabilizing layer of SC. High [Ca^{2+}] will tend to cause strong droplet aggregation and even droplet coalescence within these regions and these are probably origin of the reversal of the inhibition of phase separation by droplets. In this respect, the recent study of Antonov and Moldenaers (2011) is relevant, where phase separation of a SC + alginate + dextran system was studied as a function of particle size and charge. Large SC + dextran sulfate particles (larger than system network holes) accumulated in the SC phase and decreased SC compatibility with alginate (i.e., enhanced phase separation) due to excluded volume interactions between the alginate and the particles. Smaller nanoparticles did not appreciably affect the phase separation. On the other hand, when high [Ca^{2+}] conditions cause more extensive droplet aggregation, there will be less particles available to “block” the interface between the SC- and xanthan-rich regions, although there was no direct evidence of this from the confocal micrographs. For this

reason, attempts were made to measure any specific structuring of droplets at the water–water interface via interfacial viscosity measurements, described below.

3.3.3. Interfacial shear viscosities of the interface with oil droplets.

Fig. 3-7 shows the effects of oil composition on the apparent interfacial shear viscosity η_i between the SC-rich and xanthan-rich phases that separated from 4% w/w SC + 0.1% w/w xanthan + 1% w/w oil + 32 mM [Ca^{2+}]. The value of θ_0 for the disk submerged in the SC-rich phase was equivalent to η_i = 0.2 mN s m^{-1}, while for the xanthan-rich phase it was 2.8 mN s m^{-1}; that is, the bulk viscous drag on the disk was greater from the latter phase. Therefore, the value of θ_0 for xanthan was used to subtract for the effect of the bulk phases on the deflection of the disk. Although this is somewhat arbitrary, it is seen from eq 3-2 and the results in Fig. 3-7 that in the presence of the droplets θ_i was at least 8× larger than θ_0, so that the effect on the calculated value of η_i is negligible. It is seen that all three types of droplets, the purely liquid TD droplets (0%

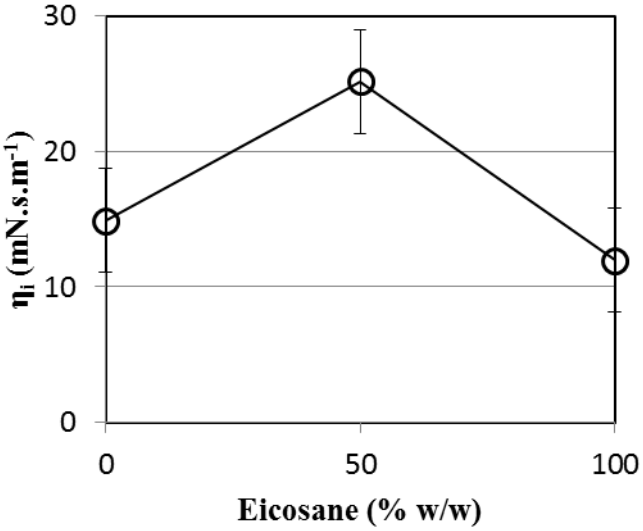

Fig. 3-7. Variation of the interfacial shear viscosity (η_i) at the macroscopic interface formed from 4% w/w SC + 0.1% w/w xanthan + [Ca^{2+}] = 32 mM + 0.75% w/w emulsion droplets as a function of the weight % eicosane in the droplets.

w/w EC), the semisolids (50% w/w EC), and the totally solid (100% w/w EC) droplets increased η_i considerably, although a distinct maximum is seen for the semisolid droplets. At $[Ca^{2+}]$ = 22 mM the mixed system gave the greatest inhibition of phase separation, and it is assumed that the maximum value of η_i is due to partial coalescence of such droplets at the water–water interface. However, it should be noted that these η_i measurements were made at the higher $[Ca^{2+}]$ = 32 mM (where inhibition was not observed) in order to have complete separation of the phases and construct the macroscopic water–water interface. Consequently, it could be that η_i is even more enhanced by the mixed droplet system at $[Ca^{2+}]$ = 22 mM.

I am currently investigating ways of measuring the relaxation of the shape of SC-rich regions that in the future may allow me to extract information on η_i and γ of the microscopic interface. Partial coalescence of oil droplets is usually observed at an intermediate solid fat content, so it makes sense that the 50:50 mixture gives the highest η_i, while the optimum solid fat content for stabilization via partial coalescence can be highly dependent on the size and morphology of the fat crystals (Fredrick, Walstra, & Dewettinck, 2010). Allen, Murray, and Dickinson (2008a) have shown that, on whipping up acidified mixed emulsions of TD and EC, optimum increases in bulk shear modulus occur above 50 to 60% EC, indicative of a partial coalescence mechanism, although this is of course for the droplets at an air–water interface.

In the absence of further information, the question remains why oil droplets accumulate at the water–water interface in the first place. Murray, Dickinson, and Wang (2009) studied the effect of 0.25 vol % 1-bromohexadecane droplets on η_i of 1% w/w SC at pH 7 at the air–water interface and found that the droplets caused a significant increase in η_i to similar values (ca. 20 mN s m^{-1}) as those measured here. Since this oil has a density very close to that of water, this increase was not due simply to creaming of the droplets to the interface. Deliberate aggregation of the droplets via acidification caused higher values of η_i. Thus it appears that droplets tend to aggregate at other

interfaces and where this occurs η_i increases. Balakrishnan, Nicolai, Benyahia, and Durand (2012) showed that latex particles with a radius as small as 0.1 μm could become trapped at the interface between the PEO- and dextran-rich phases at γ measured as low as 10^{-3} mN m^{-1}. The droplets studied in my work were even larger than this, while γ might be expected to be similar (Antonov, Puyvelde, & Moldenaers, 2004), so that these conditions might still combine to give a high enough ΔG_d via eq 3-1.

References

Allen, K. E., Murray, B. S., & Dickinson, E. (2008a). Development of a model whipped cream: Effects of emulsion droplet liquid/solid character and added hydrocolloid. *Food Hydrocolloids*, *22*, 690−699.

Allen, K. E., Murray, B. S., & Dickinson, E. (2008b). Whipped cream-like systems based on acidified caseinate-stabilized oil-in-water emulsions. *Int. Dairy J.*, *18*, 1011−1021.

Antonov, Y. A. & Moldenaers, P. (2011). Particle-destabilized semidilute biopolymer mixtures. *Soft Matter*, *7*, 2144−2149.

Antonov, Y. A., Puyvelde, P. V., & Moldenaers, P. (2004). Interfacial tension of aqueous biopolymer mixtures close to the critical point. *Int. J. Biol. Macromol.*, *34*, 29−33.

Balakrishnan, G., Nicolai, T., Benyahia, L., & Durand, D. (2012). Particles trapped at the droplet interface of water in water emulsions. *Langmuir*, *28*, 5921−5926.

Binks, B. P. & Horozov, T. S. (2006). Eds. Colloidal Particles at Liquid Interfaces; Cambridge University Press: Cambridge, U.K..

Burgaud, I., Dickinson, E., & Nelson, P. V. (1990). An improved highpressure homogenizer for making fine emulsions on a small scale. *Int. J. Food Sci. Technol.*, *25*, 39−46.

Butler, M. F. & Heppenstall-Butler, M. (2003). Phase separation in gelatin/dextran and gelatin/maltodextrin mixtures. *Food Hydrocolloids*, *17*, 815−30.

Cheng, H.-L. & Velankar, S. S. (2009). Controlled jamming of particleladen interfaces using a spinning drop tensiometer. *Langmuir*, *25*, 4412−4420.

Clegg, P. S. & Cates, M. E. (2008). Bijels: a new class of soft materials. *Soft Matter*, *4*, 2132−2138.

Clegg, P. S., Herzig, E. M., Schofield, A. B., Egelhaaf, S. U., Horozov, T. S., Binks, B. P., Cates, M. E., & Poon, W. C. K. (2007). Emulsification of partially miscible liquids using colloidal particles: Nonspherical and extended domain structures. *Langmuir, 23*, 5984−5994.

Dickinson, E. (2010). Food emulsions and foams: Stabilization by particles. *Curr. Opin. Colloid Interface Sci., 15*, 40−49.

Dickinson, E. (2011). Mixed biopolymers at interfaces: Competitive adsorption and multilayer structures. *Food Hydrocolloids, 25*, 1966−1983.

Dickinson, E. (2012). Use of nanoparticles and microparticles in the formation and stabilization of food emulsions. *Trends Food Sci. Technol., 24*, 4−12.

Dickinson, E. (2013). Stabilising emulsion-based colloidal structures with mixed food ingredients. *J. Sci. Food Agric., 93,* 710−721.

Firoozmand, H., Murray, B. S., & Dickinson, E. (2009). Interfacial structuring in a phase-separating mixed biopolymer solution containing colloidal particles. *Langmuir, 25*, 1300−1305.

Fredrick, E., Walstra, P., & Dewettinck, K. (2010). Factors governing partial coalescence in oil-in-water emulsions. *Adv. Colloid Interface Sci., 153*, 30−42.

Frith, W. J. (2010). Mixed biopolymer aqueous solutions – phase behaviour and rheology. *Adv. Colloid Interface Sci., 161*, 48−60.

Garti, N., Aserin, A., Tiunova, I., & Binyamin, H. (1999). Double emulsions of water-in-oil-in-water stabilized by alpha-form fat microcrystals. Part 1: Selection of emulsifiers and fat microcrystalline particles. *J. Am. Oil Chem. Soc., 76*, 383−389.

Ghosh, S., & Rousseau, D. (2011). Fat crystals and water-in-oil emulsion stability. *Curr. Opin. Colloid Interface Sci., 16*, 421−431.

Gupta, R. & Rousseau, D. (2012). Surface-active solid lipid nanoparticles as Pickering stabilizers for oil-in-water emulsions. *Food Funct., 3*, 302−311.

Hanazawa, T. & Murray, B. S. (2014). The influence of oil droplets on the phase separation of protein-polysaccharide mixtures. *Food Hydrocolloids*, *34*, 128-137.

Herzig, E. M., White, K. A., Schofield, A. B., Poon, W. C. K., & Clegg, P. S. (2007). Bicontinuous emulsions stabilized solely by colloidal particles. *Nat. Mater.*, *6*, 966−971.

Hore, M. J. A. & Laradji, M. (2007). Microphase separation induced by interfacial segregation of isotropic, spherical nanoparticles. *J. Chem. Phys.*, *126*, 244903.

Jansen, F. & Harting, J. (2011). From bijels to Pickering emulsions: A lattice Boltzmann study. *Phys. Rev. E*, *83*, 046707.

Krägel, J., Derkatch, S. R., & Miller, R. (2008). Interfacial shear rheology of protein-surfactant layers. *Adv. Colloid Interface Sci.*, *144*, 38−53.

Laradji, M. (2004). Langevin dynamics study of mobile filler particles in phase-separating binary systems. *J. Chem. Phys.*, *120*, 9330−9334.

Moschakis, T., Murray, B. S., & Dickinson, E. (2005). On the kinetics of acid sodium caseinate gelation using particle tracking to probe the microrheology. *J. Colloid Interface Sci.*, *284*, 714−728.

Moschakis, T., Murray, B. S., & Dickinson, E. (2006). Particle tracking using confocal microscopy to probe the microrheology in a phaseseparating emulsion containing nonadsorbing polysaccharide. *Langmuir*, *22*, 4710−4719.

Murray, B. S. (2002). Interfacial rheology of food emulsifiers and proteins. *Curr. Opin. Colloid Interface Sci.*, *7*, 426−431.

Murray, B. S. (2007). Stabilization of bubbles and foams. *Curr. Opin. Colloid Interface Sci.*, *12*, 232−241.

Murray, B. S., Dickinson, E., & Wang, Y. (2009). Bubble stability in the presence of oil emulsion droplets: influence of surface shear versus dilatational rheology. *Food Hydrocolloids*, *23*, 1198−1208.

Murray, B. S., Durga, K., Yusoff, A., & Stoyanov, S. D. (2011). Stabilization of foams and emulsions by mixtures of surface active food-grade particles and proteins. *Food Hydrocolloids*, *25*, 627−638.

Poortinga, A. T. (2008). Microcapsules from self-assembled colloidal particles using aqueous phase-separated polymer solutions. *Langmuir*, *24*, 1644−1647.

Puyvelde, P. V., Antonov, Y. A., & Moldenaers, P. (2002). Rheo-optical measurement of the interfacial tension of aqueous biopolymer mixtures. *Food Hydrocolloids*, *16*, 395−402.

Safouane, M., Langevin, D., & Binks, B. P. (2007). Effect of particle hydrophobicity on the properties of silica particle layers at the air−water interface. *Langmuir*, *23*, 11546−11553.

Scholten, E., Sagis, L. M. C., & van der Linden, E. (2006). Effect of bending rigidity and interfacial permeability on the dynamical behaviour of water-in-water emulsions. *J. Phys. Chem. B*, *110*, 3250−3256.

Simeone, M., Alfani, A., & Guido, S. (2004). Phase diagram, rheology and interfacial tension of aqueous mixtures of Na-caseinate and Naalginate. *Food Hydrocolloids*, *18*, 463−470.

Stratford, K., Adhikari, R. I., Pagonabarraga, I., Desplat, J.-C., & Cates, M. E. (2005). Colloidal jamming at interfaces: A route to fluidbicontinuous gels. *Science*, *309*, 2198−2201.

Tolstoguzov, V. B. In Functional Properties of Food Macromolecules; Mitchell, J. R., Ledward, D. A., Eds.; Elsevier Applied Science: London, 1986; p 385.

Tromp, R. H., Rennie, A. R., & Jones, R. A. L. (1995). Kinetics of the simultaneous phase-separation and gelation in solutions of dextran and gelatin. *Macromolecules*, *28*, 4129−4138.

White, K. A., Schofield, A. B., Binks, B. P., & Clegg, P. S. (2008). Influence of particle composition and thermal cycling on bijel formation. *J. Phys. - Condens. Matter*, *20*, 494223.

Williams, M. A. K., Fabri, D., Hubbard, C. D., Lundin, L., Foster, T. J., Clark, A. H., Norton, I. T., Lorén, N., & Hermansson, A.-M. (2001). Kinetics of droplet growth in gelatin/maltodextrin mixtures following thermal quenching. *Langmuir*, *17*, 3412−3418.

Wolf, B., Scirocco, R., Frith, W. J., & Norton, I. T. (2000). Shear-induced anisotropic microstructure in phase-separated biopolymer mixtures. *Food Hydrocolloids*, *14*, 217−225.

Chapter 4

Effects of solid fat content in fat particles on their adsorption at the air–water interface

4.1. Introduction

Bubbles play an important role in food, delivering a desirable mouthfeel, texture, appearance and sometimes flavour. For example, the CO_2 bubbles in beer contribute to providing a refreshing and invigorating product, and air bubbles impart the light and smooth texture to ice cream despite the fact that it is frozen (Dickinson, 1992). However, the difference in Laplace pressure between bigger and smaller bubbles causes bubbles to quickly disappear if no stable membrane structure occurs at their interface. Therefore, bubbles in foods are stabilised by small molecule emulsifiers, proteins and other particles, with their degree of stability affected by the interfacial structure of these materials at the air–water interface.

In whipped cream and ice cream, electron microscopy reveals that fat particles accumulate at the air–water interface and compose the interfacial structure (Anderson & Brooker, 1988). The typical whipping process of dairy cream consists of three steps (Anderson & Brooker, 1988; Besner & Kessler, 1998; Fredrick et al., 2013; Hotrum, Cohen Stuart, van Vliet, Avino, & van Aken, 2005, Jakubczyk & Niranjan, 2006; Needs & Huitson, 1991; Noda & Shiinoki, 1986; van Aken, 2001). First, a protein membrane forms at the air–water interface. After the large bubbles form with a bare interface through whipping, proteins, such as α-casein, β-casein and whey proteins, are rapidly adsorbed at the newly-produced air–water interface via diffusion, causing a decrease in the interfacial tension. In the second stage, the large bubbles are further sheared to produce small bubbles, by spreading the area of the air–water interface. The

newly-formed interfacial membrane mainly consists of fat particles or their aggregates. If fat crystals stick through the oil–water interface membrane, the bridging between air bubbles and fat particles is facilitated. After fat particles are adsorbed at the air–water interface, some lose their shape (Brooker, Anderson, & Andrews, 1986; Needs & Huitson, 1991), and other fat particles will form an interfacial network structure, followed by the spreading of inner oil at the air–water interface (Hotrum, Cohen Stuart, van Vliet, & van Aken, 2004). This process is called surface-mediated partial coalescence. In the third stage, a network structure is formed by fat particles aggregating in the serum. At the same time, some aggregated fat particles that have been adsorbed at the air–water interface in the second stage are released from the interface due to the shrinking of the surface area. Those fat particles and fat clumps promote bubble association, resulting in the formation of a network structure via connected bubbles in the serum phase. This structure, which is composed of bubbles and fat globules, gives viscosity and firmness to whipped cream and maintains the whipped cream's shape.

Generally, the solid fat content (SFC) in fat particles has a great impact on aggregation via partial coalescence (Boode & Walstra, 1993). If the majority of the fat is solid, the fat particles are very stable against shearing forces. If the fat particles are composed of liquid oil, the particles are also stable, and normal coalescence may occur. However, if fat particles contain some amount of fat crystals, the particles are connected to each other via the fat crystals, leading to partial coalescence. There are several papers demonstrating that such partial coalescence is maximised when the SFC is in the range of approximately 10–50% (Davies, Dickinson, & Bee, 2000). For example, Boode and Walstra (1993) simulated the aggregation of fat particles under shearing and revealed that coalescence was facilitated when the SFC exceeded 12%. Hinrichs and Kessler (1997) investigated the stability of dairy cream under shearing with SFC in the range of 25–65% and found the system was most unstable when the SFC reached 25%. Typically,

the SFC in commercial dairy cream is less than 40% when whipped (Needs & Huitson, 1991).

Recombined cream, which is composed of vegetable oils and emulsifiers, is suitable for studying the effects of solid fat on partial coalescence because SFC is easily controlled by adding vegetable oils. Fuller et al. (2015) prepared recombined cream with hydrogenated palm kernel oil, canola oil, sodium caseinate and Tween 20 to examine the effect of SFC and interfacial composition of the oil–water interface on cream stability. Mutoh, Nakagawa, Noda, Shiinoki, and Matsumura (2001) prepared recombined creams using three kinds of vegetable oils with different SFC profiles and investigated the solidification of the creams that occurred after a short thermal treatment, followed by cooling to the chilled state. The results showed that the solidification of the cream after the thermal treatment occurred via partial coalescence when the SFC of the cream was between 11 and 13%.

The physical properties of interfacial layers are often measured to monitor the adsorption process of compounds, such as surfactants and particles, to gain information about their interfacial structure. The interfacial tension and shear viscosity measured by previous investigators revealed the competitive adsorption of protein–protein and protein–low molecular emulsifiers at air–water and oil–water interfaces (Courthaudon, Dickinson, & Dalglesh, 1991; Dickinson & Iveson, 1993; Dickinson, Murray, & Stainsby, 1985; Dickinson, Rolfe, & Dalgleish, 1990; Murray, Færgemand, Trotereau, & Ventura, 1999). Other researchers determined the adsorption of fat particles onto the protein interface layer and the spreadability of fat at the air–water interface, by measuring the interfacial tension with Wilhelmy plate-type equipment (Hotrum, van Vliet, Cohen Stuart, & van Aken, 2002; Hotrum, Cohen Stuart, van Vliet, & van Aken, 2003, 2004). These results were related to the authors whipping process model (Hortum et al., 2005). Cheng and Velankar (2009) used the droplet relaxation technique to focus specifically on particle-jamming effects in oil–water systems. A dilatational rheology

apparatus has been used for studies of oil–water and air–water interfaces (Benjamins, Cagna, & Lucassen-Reynders, 1996; Benjamins, Lyklema, & Lucassen-Reynders, 2006; Burke, Cox, Petkov, & Murray, 2014; Chen et al., 2017; Li et al., 2018; Mezdour, Desplanques, & Relkin, 2011; Tamm & Drusch, 2017). Wouters et al. (2018) studied the formation and interfacial characteristics of mixed gluten hydrolysate and egg white protein solutions. From the results, it was hypothesised that the egg white protein forms a secondary protein layer below the air–water interface that is maintained by gluten hydrolysate constituents. For the adsorption of oil droplets at the air–water interface, Murray, Dickinson, and Wang (2009) observed an increase in the initial viscoelastic modulus of the protein layer at the air–water interface with *n*-tetradecane particles above pH 5.5 and found that the interfacial shear viscosity correlated well with the bubble stability. In some studies, the time-dependent changes of the interfacial tension and viscoelastic modulus have been used to reflect the protein and polysaccharide adsorption process and the structure formation at the oil–water and air–water interfaces, respectively (Benjamins et al., 1996, 2006; Fuentes-Prado & Martínez-Padilla, 2014; Peng et al., 2018; Tamm & Drusch, 2017; Wouters et al., 2018). Fuentes-Prado and Martínez-Padilla (2014) studied thermo-acidic treated wheat gluten as a forming agent by measuring the interfacial tension and dilatational rheology of the air–water interface. Jara, Sánchez, Patino, and Pilosof (2014) analysed the adsorption behaviour of proteins and hydroxypropylmethylcellulose at the air–water interface by measuring the interfacial pressure and dilatational elasticity. The results of the time-dependent change in interfacial pressure and dilatational elasticity distinctly show the effect of pH on the competitive adsorption behaviour of protein and hydroxypropylmethylcellulose, as well as the interfacial film properties. Peng et al. (2018) examined the adsorption of gliadin nanoparticles onto the air–water interface, by measuring the time-dependent changes in interfacial tension and dilatational rheology. The results suggest that the zeta-potential played a leading role in the adsorption rate of gliadin nanoparticles onto the air–water

interface, whereas particle size and morphology did not.

As described above, it is known that fat crystals in fat particles cause partial coalescence, thereby affecting the stability and texture of whipped cream. However, it remains unclear how fat crystals contribute to the process of fat particle adsorption to the air–water interface and the following structural formation in the adsorbed layer. This study aims to investigate how solid fat in creams affects the process of fat particle adsorption and the establishment of interfacial structures at the air–water interface. Three kinds of vegetable oil with different SFC profiles were used for comparison. These oils were emulsified with a sodium caseinate solution to create the three creams used for the experiments. The effects of fat particle content on interfacial tension and dilatational viscoelastic modulus at the air–water interface were examined at different temperatures using a dilatational rheology measurement technique. Electron microscopy was undertaken to observe the adsorbed layer at the surface of the air bubbles incorporated into the creams due to whipping.

4.2. Materials and methods

4.2.1. Materials

Sodium caseinate was bought from Arla Foods Ingredients Amba (Miprodan 31, Aarhus, Denmark), and imidazole and HCl were procured from Wako Pure Chemical Industries, Ltd. (Osaka, Japan). Three kinds of vegetable oil with different SFC profiles were used (Fig. 4-1). The major fatty acids in Fats A and B were lauric acids. Fat B was purchased from Fuji Oil Co., Ltd. (Osaka, Japan). Fat A was prepared through the hydrogenation of Fat B to change its melting point. Fat C, whose predominant fatty acid was oleic acid, was prepared by mixing Fat B with soybean oil (Nisshin OillO Group, Ltd., Tokyo, Japan) and hydrogenated soybean oil.

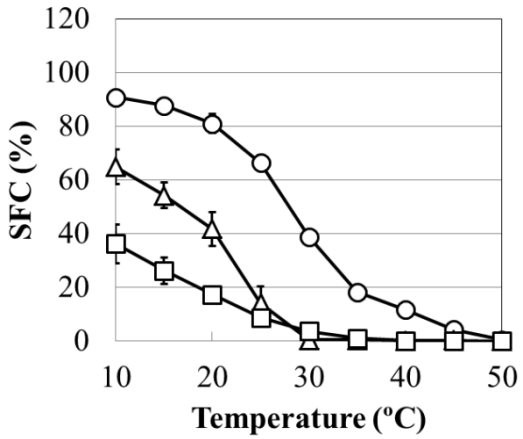

Fig. 4-1. The solid fat content (SFC) versus temperature for Fat A (○), Fat B (△) and Fat C (□).

4.2.2. Cream preparation

Sodium caseinate was dissolved in a 20 mM imidazole-HCl buffer (pH 7.0) by stirring overnight (Rexim RSH-6DH, As One Co., Osaka, Japan). Vegetable oils were kept at 65 °C in a water bath for 2 h to melt all fat crystals. The sodium caseinate solution and oil were mixed at 65 °C and 10,000 rpm in a high-speed blender (NS-51, Nitti-On Co., Ltd., Chiba, Japan) with an NS-30U stirring blade (Nitti-On Co., Ltd., Chiba, Japan), for 3 min. The oil-in-water (O/W) emulsions contained 2% w/w sodium caseinate and 40% w/w fat. The emulsions were homogenised twice in two stages with a high-pressure homogeniser (Panda Plus 2000, GEA Niro Soavi, Parma, Italy) using 9 MPa pressure for the first stage and 1 MPa for the second. The prepared O/W emulsions were kept in a vessel and cooled to 4 °C with ice water, then placed in a refrigerator at 4 °C overnight. The emulsions that included Fat A, B and C were named Cream A, B and C, respectively. These 40% w/w creams were diluted to 10–30% w/w creams using the 2% w/w sodium caseinate solution. The average diameters d_{32} of fat particles in these creams were measured by a laser diffraction particle size analyser (SALD-2300, Shimadzu Co., Kyoto, Japan) and found to be 1.7 ± 0.2 μm.

4.2.3. SFC measurement

The SFC in creams between 10 and 40 °C was estimated by a pulsed nuclear magnetic resonance (NMR) spectrometer (Minispec mq20, Bruker Co., MA, USA). A standard daily check was performed through calibration with three supplied standards, containing 0.0, 32.3 and 73.4% SFC. Approximately 2 mL of the creams was placed in acclimatised glass tubes and kept at each temperature for 30 min, before the measurement. The SFC value was determined by the direct method installed on the NMR spectrometer. Given the measurements were performed for 40% w/w cream, the SFC in the fat particles was taken to be 2.5-fold the SFC in the whole emulsion.

4.2.4. Interfacial tension and dilatational modulus measurement of air–water interface

The interfacial tension and dilatational modulus at the air–water interface were estimated using a dynamic drop tensiometer manufactured by Teclis-IT Concept (Longessaigne, France), as described previously (Benjamins et al., 1996, 2006).

Interfacial tension, γ, was calculated by applying the Young-Laplace equation to the drop profile:

$$\Delta p = \gamma[(1/r_1) + (1/r_2)] \quad (4\text{-}1)$$

where Δp is the pressure difference between the air and water, and r_1 and r_2 are the principal radii of the curvature.

The instrument can also evaluate the measured sinusoidal oscillations of the interfacial tension by applying the Young–Laplace equation to the shape of the oscillating drop. The dilatational modulus, |E|, is simply derived from the amplitudes of the oscillations $\Delta\gamma$ and ΔA by:

$$|E| = A(\Delta\gamma/\Delta A) \quad (4\text{-}2)$$

where A is the interfacial area.

The elastic modulus E' and viscous modulus E" are calculated from |E| and the phase angle φ between $\Delta\gamma$ and ΔA:

$$E' = |E|\cos\varphi \quad (4\text{-}3)$$

$$E'' = |E|\sin\varphi \quad (4\text{-}4)$$

The creams that included 10–40% w/w fat and 2% w/w sodium caseinate were diluted 10,000 times in 20 mM imidazole-HCl buffer (pH 7.0) because highly transparent sample creams were necessary for measurements. The diluted creams were kept in a water bath whose temperature was set to the measurement temperature. The temperature of the cuvette in the apparatus was controlled by circulating the water from a water bath (F12-ED, Julabo Japan Co., Ltd, Osaka, Japan) and kept for more than 1 h before the measurement. The diluted creams were added to an optical glass cuvette, and air bubbles with an interface area of 15 mm^2 were penetrated in the continuous water phase with an 18-gauge raised needle (Teclis-IT Concept). Interfacial tension was measured continuously while keeping the surface area 15 mm^2 throughout the measurement. The interfacial viscoelastic modulus was measured every 320 s. The $\Delta A/A$ was 0.1, and the frequency of the oscillation was 0.1 Hz. Measurement continued until the interfacial tension reached a constant value. The measurement lengths were approximately 240 min at 10 °C, 170 min at 20 °C, 120 min at 30 °C and 70 min at 40 °C. The measurements at each temperature were repeated three times and averaged.

4.2.5. Microstructure observation of the air–water interface

Cryo-scanning electron microscopy (cryo-SEM; S4100, Hitachi, Ltd., Tokyo, Japan) was used to observe the microstructure of the air–water interface with and without fat particles. Creams and sodium caseinate solution were kept at 10 °C before whipping and were whipped with a hand mixer (Dendo Mini Creamer, Eko Kinzoku Co., Ltd., Niigata, Japan) at room temperature for 1 min. Whipped creams were placed into straws, which were cut to 1 cm length and fixed on the observation platform of the microscopy by OCT compound (Sakura Finetek Japan Co., Ltd., Tokyo, Japan), and cooled rapidly with slush nitrogen for 30 s. The iced creams on the platform were set

into the sample chamber for microscopy and cut by the iced knife placed in the chamber. Iced water was sublimed by raising the temperature in the chamber to -90 °C, and gold was deposited on the sample surface. The microstructures of whipped creams were observed at 1.5 kV acceleration voltage.

4.3. Results and discussions

4.3.1. SFCs of fat in creams

The SFCs in creams between 10 and 40 °C are shown in Fig. 4-2. Cream A contained 100.0% SFC below 20 °C, 50.4% at 30 °C and 12.6% at 40 °C. Cream B contained 76.0% SFC at 10 °C and 33.9% SFC at 20 °C, but the fat became liquid above 30 °C. Conversely, Cream C contained 28.4% SFC at 10 °C, 13.1% SFC at 20 °C, 1.4% SFC at 30 °C and 0.0% SFC at 40 °C. Thus, the trends were approximately similar to those for vegetable oil, where the highest SFC was for Cream A, followed by B and C, except at 30 °C, where SFC in Cream C (1.4%) was higher than that in Cream B (0.2%).

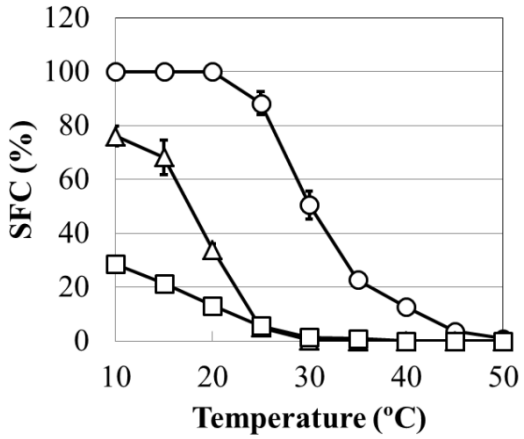

Fig. 4-2. The solid fat content (SFC) versus temperature in Cream A (○), Cream B (△) and Cream C (□).

4.3.2. Effects of fat particles on interfacial tension and dilatational modulus of air–water interface

Time-dependent changes of interfacial tension and dilatational modulus for sodium caseinate solution (2% w/w protein) and Cream B (2% w/w protein, 40% w/w fat) show the typical result of interfacial tension and dilatational modulus measurements (Fig. 4-3). The measurement temperature was 20 °C. The sodium caseinate solution and

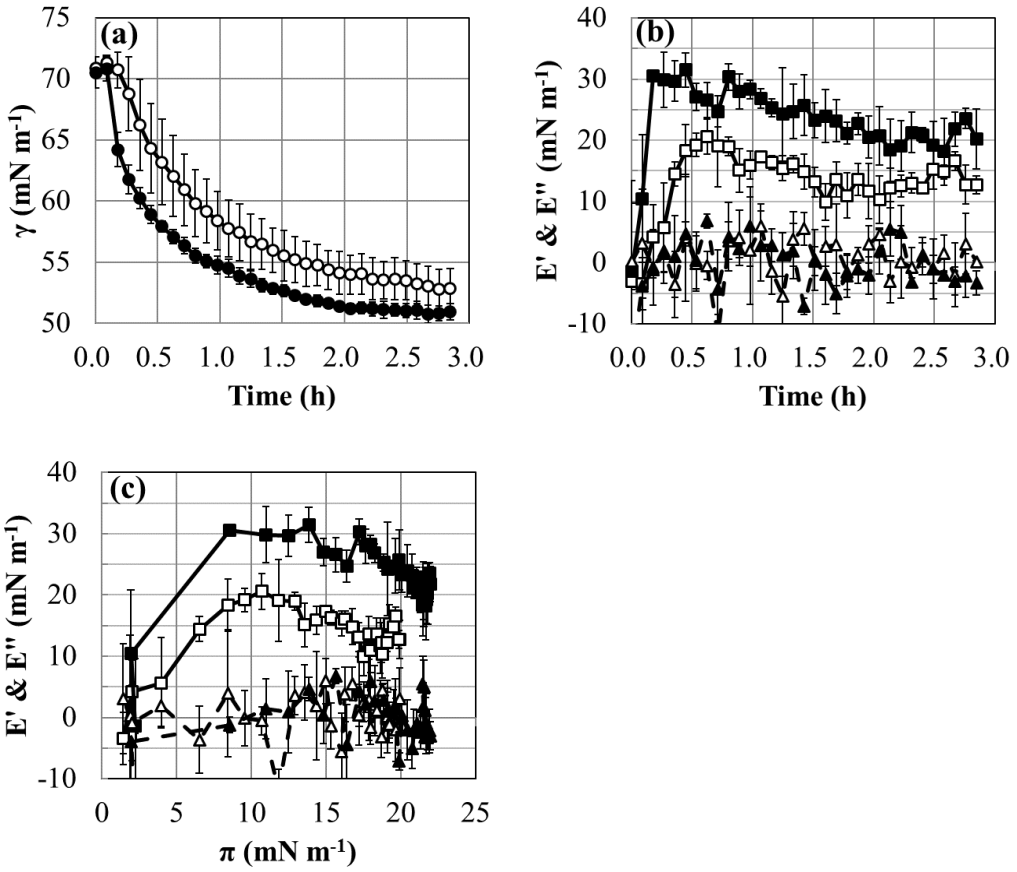

Fig. 4-3. Interfacial parameters of air–water interfaces, containing sodium caseinate and Cream B at 20 °C. (a) Interfacial tension (γ) as a function of time; (b) interfacial elastic modulus (E') and interfacial viscous modulus (E") as a function of time; (c) E' and E" as a function of surface pressure (π): γ (○), E' (□) and E" (△), for 2% w/w sodium caseinate solution diluted 10,000-fold; γ (●), E' (■) and E" (▲), for Cream B containing 40% w/w fat and 2% w/w sodium caseinate, diluted 10,000-fold.

Cream B were diluted 10,000 times just before the measurements, as described in the methods. Fig. 4-3(a) shows the time-dependent changes of interfacial tension, γ. The presence of fat particles (Cream B) caused a faster decrease of γ and lower values of γ at the end. This behaviour means that fat particles covered by sodium caseinate adsorb more efficiently than free sodium caseinate. Fig. 4-3(b) illustrates the changes in interfacial elastic modulus (E') and viscous modulus (E") with time. For diluted 2% w/w sodium caseinate, E' increased to ca. 20 mN m^{-1}, and E' of diluted Cream B containing 40% w/w fat increased above 30 mN m^{-1}, while E" with and without fat particles was ca. 0 mN m^{-1} throughout the measurements. The E" values of all other experiments were ~0 mN m^{-1}, regardless of fat type and content (data not shown). These results indicate that the interfacial layers formed by adsorbed sodium caseinate and fat particles in this study are highly elastic. Cream B had a higher E' than sodium caseinatesolution throughout the measurements, suggesting that the fat particles build up the films at the air–water interface more rigidly than those by sodium caseinate.

Fig. 4-3(c) depicts E' and E" versus surface pressure, π, which is calculated by subtracting γ across time from that for the pure air–water interface. The surface pressure is thought to be an index of adsorption level. Therefore, this plot can be compared directly with the E' and E" of sodium caseinate solution and Cream B, at the same adsorption level. Fig. 4-3(c) demonstrates that E' of Cream B increased more than that of sodium caseinate solution, at the same adsorption level. Hotrum, van Vliet, Cohen Stuart and van Aken (2002) reported that oil droplets could enter and spread at the air–water interface when the surface pressure is below a critical value. The critical value of the sunflower oil/protein solution (whey protein or sodium caseinate)/air system is 15 mN m^{-1}. In my result, the difference in E' between the sodium caseinate solution and Cream B was observed just after the start of the measurement, when the surface pressure was below 15 mN m^{-1}, which may facilitate the adsorption of fat particles to the air–water interface. The E' of sodium caseinate solution and Cream B decreased

with increased surface pressure after E' had reached its maximum value. Similar results were observed for adsorbed films of sodium caseinate at the oil–water and air–water interfaces (Benjamins et al., 1996, 2006; Noskov, Latnikova, Lin, Loglio, & Miller, 2007; Ridout, Mackie, & Wilde, 2004). Sodium caseinate is composed of four kinds of proteins, α_{s1}-, α_{s2}-, β- and κ-casein, among which β-casein is highly surface-active (Walstra, Wouters, & Geurts, 2006). Adsorbed β-casein structure at the air–water interface seems to change with increasing areal density of β-casein (Dalgleish, 1997). First, the entire molecule of β-casein occupies the interface, but the excess adsorption may cause the re-orientation of the molecule to make hydrophilic chains extend to the aqueous phase. Such re-orientation or re-arrangement may be responsible for the decrease of the interfacial modulus after the maximum point. This mechanism should work for sodium caseinate adsorption at the interface, in the current experiment. However, despite the difference in modulus levels, similar patterns were observed for sodium caseinate solution and Cream B, suggesting that the basic structure of the protein layer should be maintained, even when fat particles of Cream B are adsorbed to the air–water interface layer. In other words, fat particles can strengthen the interfacial layer without damaging the protein network.

The interfacial elastic membrane should be formed quickly to stabilise against Ostwald ripening because bubbles in food without interfacial membranes disappear rapidly (Dickinson, 1992). Therefore, the adsorption speed of macromolecules or particles to the air–water interface, which caused an increase of elastic modulus of the interface, must be important for the whipping process. Fig. 4-4(a) provides the time-dependent changes of γ for the sodium caseinate solution at different temperatures, from 10 to 40 °C. The result at 20 °C is the same as that in Fig. 4-3(a). Fig. 4-4(b) is the time-dependent changes of γ for 40% w/w Cream B. The result at 20 °C is the same as that in Fig. 4-3(a). These results show that time-dependent changes of γ were strongly affected by temperature and presence of fat particles. I think that the process of

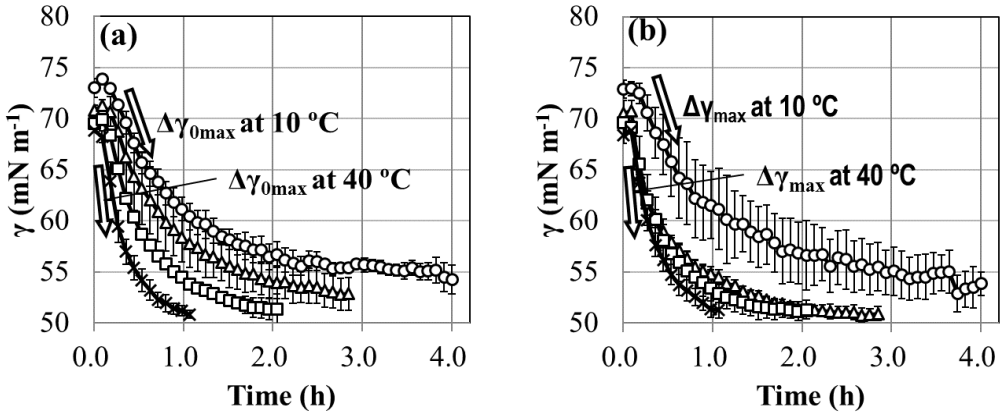

Fig. 4-4. Decreasing interfacial tension (γ) with time at 10 °C (○), 20 °C (△), 30 °C (□) and 40 °C (×): (a) 2% w/w sodium caseinate solution diluted 10,000-fold; (b) 40% w/w Cream B diluted 10,000-fold.

formation of interfacial structures at the air–water interface in cream is crucially affected by competitive adsorption of protein and fat particles. Therefore, to further evaluate the effects of fat particles on the interfacial properties from the viewpoint of the competition between fat particles and proteins (in this case, sodium caseinate), interfacial parameters at the air–water interface using creams containing 10 and 40% fat, were measured. In addition, a quantitative comparison for each temperature is needed. Thus, I calculated the maximum decline speeds for interface tension of the sodium caseinate solution, $\Delta\gamma_{0max}$, and that for diluted cream, $\Delta\gamma_{max}$, of Cream A, B and C, from all measurement results of time-dependent changes of γ.

Table 4-1 lists the calculated $\Delta\gamma_{max}$ of sodium caseinate, $\Delta\gamma_{0max}$ and that of diluted creams, $\Delta\gamma_{max}$ of Creams A, B and C. Then, $\Delta\gamma_{max}/\Delta\gamma_{0max}$ was calculated from these results to estimate the effect of the presence of fat particles on the adsorption rate to the air–water interface. For example, $\Delta\gamma_{0max}$ at 10, 20, 30 and 40 °C was 1.06±0.27, 1.05±0.20, 1.53±0.30 and 3.30±0.59 mN m^{-1} s^{-1}, respectively. Whereas, $\Delta\gamma_{max}$ of 40% w/w Cream B at the same temperatures (10, 20, 30 and 40 °C) was 1.13±0.40,

2.42±0.19, 1.97±0.30 and 1.96±0.21 mN m^{-1} s^{-1}, respectively. Therefore, $\Delta\gamma_{max}/\Delta\gamma_{0max}$ of 40% w/w Cream B at 10, 20, 30 and 40 °C were 1.07, 2.31, 1.29 and 0.59, respectively.

Fig. 4-5 reveals the calculated $\Delta\gamma_{max}/\Delta\gamma_{0max}$ for Cream A, B and C as a function of their fat content. The temperature was between 10 and 40 °C. The $\Delta\gamma_{max}/\Delta\gamma_{0max}$ of 40% w/w Cream B, calculated in the preceding paragraph, is plotted at the position of 40% w/w on the *x*-axis in Fig. 4-5(b) (indicated by arrows). Changes of $\Delta\gamma_{max}/\Delta\gamma_{0max}$ as a function of fat content at different temperatures were compared. As a result, the $\Delta\gamma_{max}/\Delta\gamma_{0max}$ of Cream B at 20 °C increased with increasing fat content, such that

Table 4-1 Calculated maximum decline speeds for interface tension of the sodium caseinate solution, $\Delta\gamma_{0max}$ and that of diluted creams, $\Delta\gamma_{max}$ of Creams A, B and C.

		Maximum decline speeds for interfacial tension (mN m^{-1} s^{-1})			
Samples	Fat content (% w/w)	10 °C	20 °C	30 °C	40 °C
Sodium caseinate	-	1.06±0.27	1.05±0.20	1.53±0.30	3.30±0.68
Cream A	10	0.64±0.14	0.90±0.08	1.70±0.33	2.51±0.86
	20	0.69±0.12	1.32±0.14	1.86±0.56	1.93±0.33
	30	1.03±0.12	1.20±0.06	1.92±0.35	2.31±0.95
	40	0.86±0.09	1.45±0.18	2.35±0.13	2.08±0.21
Cream B	10	0.90±0.22	1.11±0.18	1.39±0.15	2.13±0.69
	20	1.05±0.06	1.52±0.24	1.40±0.28	2.15±0.42
	30	1.14±0.22	1.96±0.55	1.55±0.19	2.55±0.36
	40	1.13±0.40	2.42±0.19	1.97±0.30	1.96±0.21
Cream C	10	0.96±0.16	1.23±0.02	1.24±0.22	3.55±0.40
	20	1.05±0.22	1.39±0.11	1.43±0.43	2.24±0.42
	30	1.66±0.21	1.87±0.27	1.56±0.44	2.17±0.26
	40	1.53±0.61	2.30±0.23	1.44±0.22	2.29±0.66

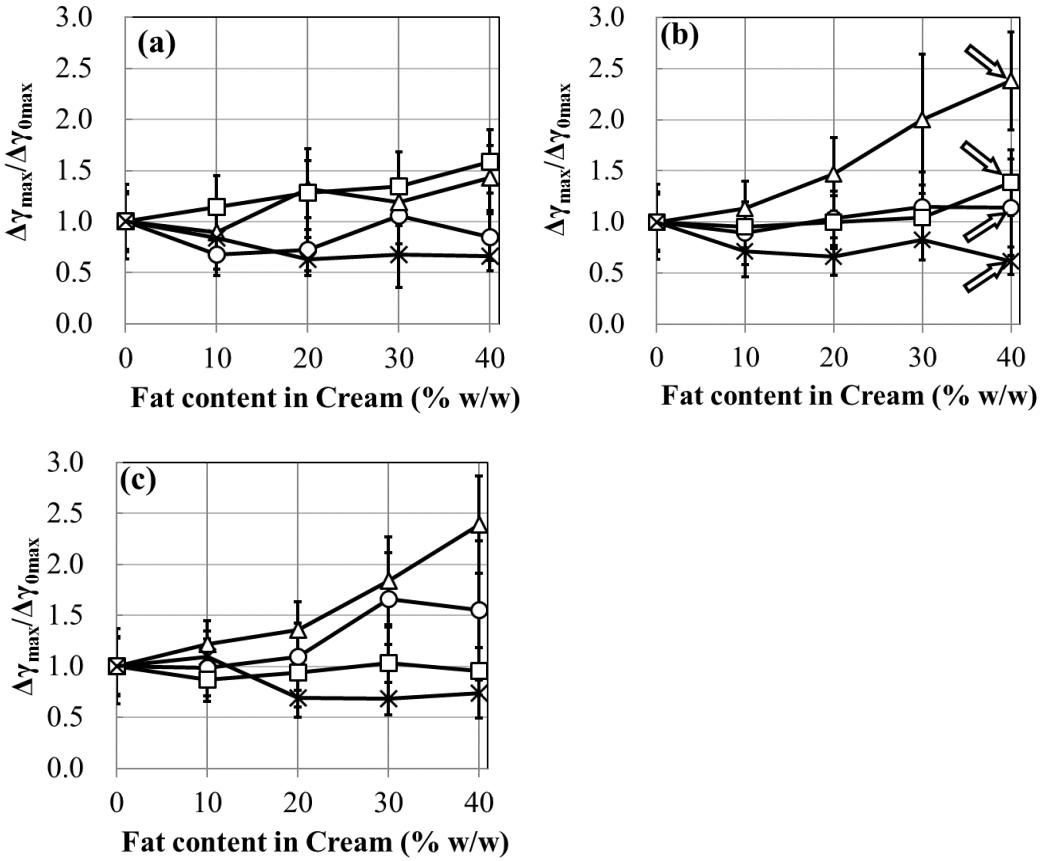

Fig. 4-5. $\Delta\gamma_{max}/\Delta\gamma_{0max}$ as a function of fat content in (a) Cream A, (b) Cream B and (c) Cream C. $\Delta\gamma_{max}/\Delta\gamma_{0max}$ is the ratio of the maximum decline speed of interfacial tension with and without fat particles: Measurements were conducted at 10 °C (○), 20 °C (△), 30 °C (□) and 40 °C (×). The arrows indicate $\Delta\gamma_{max}/\Delta\gamma_{0max}$ of 40% w/w Cream B, which was calculated using $\Delta\gamma_{max}$ and $\Delta\gamma_{0max}$, as shown in Fig. 3-4.

$\Delta\gamma_{max}/\Delta\gamma_{0max}$ reached approximately 2.31; however, significant increases were not observed at 10 or 30 °C. At 40 °C, the $\Delta\gamma_{max}/\Delta\gamma_{0max}$ of Cream B seemed to decrease with increasing fat content in the cream. Notably, the SFCs of Cream B were 33.9 and 76.0% at 20 and 10 °C, respectively, but was nearly 0.0% at 30 and 40 °C (Fig. 4-2). Similar results were observed for Cream C (Fig. 4-5(c)). The largest increase of $\Delta\gamma_{max}/\Delta\gamma_{0max}$ with increasing fat content was noted again at 20 °C. An increase, though lesser, was

also seen at 10 °C. The SFCs in Cream C at 10 and 20 °C were 28.4 and 13.1% (Fig. 4-2), respectively. The $\Delta\gamma_{max}/\Delta\gamma_{0max}$ of Cream C at 30 °C was ca. 1.00, irrespective of fat content, and the SFC in the cream was 1.4%. At 40 °C, the $\Delta\gamma_{max}/\Delta\gamma_{0max}$ of Cream C did not increase with increasing fat content but tended to decrease by less than 1.00, above 20% w/w fat content. It is worth noting that $\Delta\gamma_{max}/\Delta\gamma_{0max}$ decreased with increasing fat content at 40 °C in Cream B and Cream C, and the SFCs of both creams were 0%. From these results, an increase of $\Delta\gamma_{max}/\Delta\gamma_{0max}$ with increasing fat content for Cream B and Cream C occurred when the SFC of the cream was in this limited range. This point will be discussed below, in combination with the maximum value of the interfacial modulus, E'_{max}. Fig. 4-5(a) displays $\Delta\gamma_{max}/\Delta\gamma_{0max}$ for Cream A. The trend was different from that of Cream B and Cream C. Increases of $\Delta\gamma_{max}/\Delta\gamma_{0max}$ with increasing fat content were observed at 20 and 30 °C, but the extent of increase was smaller as compared to those of Cream B (20 °C) and Cream C (10 and 20 °C). Whereas, $\Delta\gamma_{max}/\Delta\gamma_{0max}$ of Cream A at 10 and 40 °C was nearly less than 1.00.

In addition to the value of γ, I compared the maximum value of interfacial elastic modulus, E'_{max}, to investigate the difference in strength of adsorbed layers formed by sodium caseinate and fat particles at the air–water interface. Fig. 4-6 presents the E'_{max} of Creams A, B and C as a function of fat content and at different temperatures (from 10 to 40 °C). The E'_{max} of sodium caseinate solution, that is, $E'_{0max,}$ at each temperature is shown at 0% w/w fat content in all figures. At 10, 20, 30 and 40 °C, the E'_{0max} values were 21.9±4.4, 21.2±2.4, 17.5±1.8 and 15.8±0.7 mN m^{-1}, respectively. For Cream B, E'_{max} increased as a function of fat content irrespective of the temperatures measured (Fig. 4-6(b)). Therefore, I compared E'_{max} at 40% w/w fat content. The largest value of E'_{max} was 30.6±1.9 mN m^{-1} when the measured temperature was 20 °C. At 10 and 30 °C, the measured E'_{max} values were 27.0±4.8 and 26.3±0.3 mN m^{-1}, respectively. The lowest value (19.3±0.2 mN m^{-1}) was obtained when the measured temperature was 40 °C. For Cream C, the E'_{max} tended to increase with increasing fat content at any

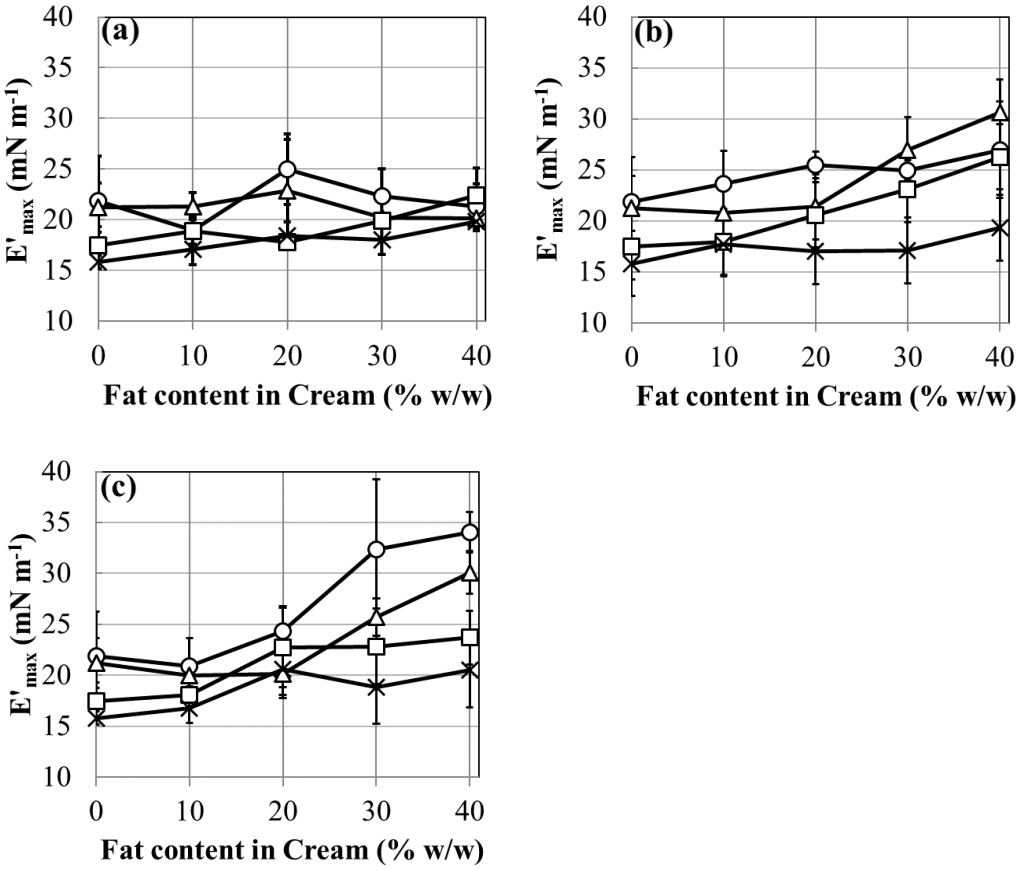

Fig. 4-6. Maximum value of interfacial elastic modulus (E'_{max}) as a function of fat content in (a) Cream A, (b) Cream B and (c) Cream C. Measurements were conducted at 10 °C (○), 20 °C (△), 30 °C (□) and 40 °C (×).

temperature (Fig. 4-6(c)), as was observed for Cream B. The highest E'_{max} was observed for 40% w/w cream at 10 °C (ca. 34.0±2.0 mN m^{-1}) while E'_{max} of Cream C at 40% w/w and 20 °C was ca. 30.1±2.1 mN m^{-1}. No increase of E'_{max} was observed at 10 and 20 °C with increasing fat content for Cream A (Fig. 4-6(a)), but E'_{max} increased slightly with increasing fat content measured at 30 and 40 °C. The trend of E' of Cream A was different from that of Cream B and Cream C, which is consistent with the results of $\Delta\gamma_{max}/\Delta\gamma_{0max}$.

To compare the effect of SFC on interfacial properties, values of $\Delta\gamma_{max}/\Delta\gamma_{0max}$

and E'_{max} of diluted 40% w/w cream were plotted as a function of SFC (Fig. 4-7). Fig. 4-7(a) suggests that $\Delta\gamma_{max}/\Delta\gamma_{0max}$ is affected by both temperature and SFC. It seems that $\Delta\gamma_{max}/\Delta\gamma_{0max}$ increased when the temperature was 20 and 10 °C, and the SFC in the fat particles was between 10 and 50%. For both Cream C (SFC 33.9%, Fig. 4-2) and Cream B (SFC 13.1%), $\Delta\gamma_{max}/\Delta\gamma_{0max}$ value at 20 °C was ca. 2.5, which was higher than that of Cream A (SFC 100%) at 20 °C. In this instance, although temperature satisfied the required condition for all the creams, the SFC of Cream A was out of the appropriate range. When comparing the results at 10 °C, $\Delta\gamma_{max}/\Delta\gamma_{0max}$ of Cream C (SFC 28.4%) was higher than those of Cream A (SFC 100.0%) and Cream B (SFC 76.0%). In this case, only the SFC of Cream C is positioned in the appropriate range from 10 to 50%. Summarising these results, I can say that the adsorption speed of fat particles to the air–water interface is accelerated when SFC is in the range between 10 and 50%. Hotrum et al. (2005) focused on the spreading behaviour of oil droplets at the air–water interface and surface-mediated particle coalescence. In their model, fat particles can attach to the protein covered air–water interface when the spreading coefficient is

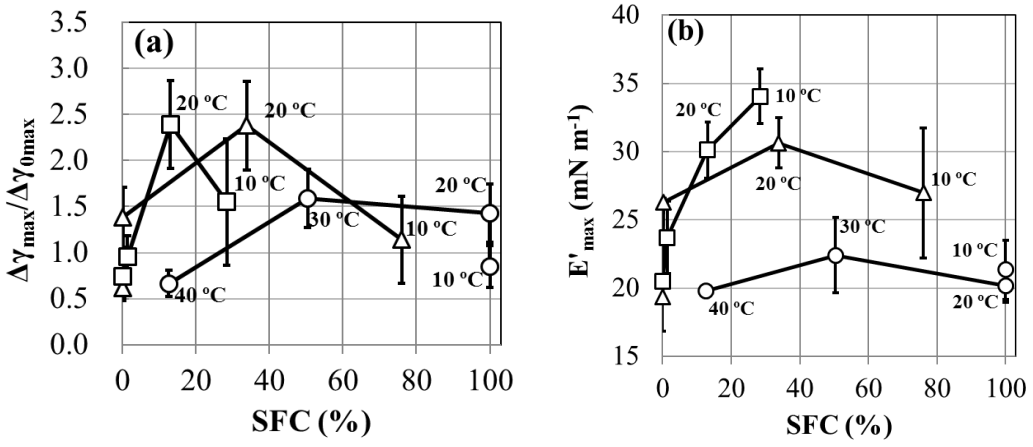

Fig. 4-7. Effects of solid fat content (SFC) on the ratio of maximum decline speed of interfacial tension ($\Delta\gamma_{max}/\Delta\gamma_{0max}$) (a) and the maximum value of interfacial elastic modulus (E'_{max}) (b) for Cream A (○), Cream B (△) and Cream C (□).

positive, which is calculated from the surface tensions at the three-phase boundary between the oil, water and air. Afterwards, interfacial flocculation occurs, which is ensured via partial coalescence of the interfacial flocculation. My results suggest that the presence of fat crystals promotes oil droplet adsorption at the air–water interface via surface-mediated partial coalescence, as evidenced by an increase of $\Delta\gamma_{max}/\Delta\gamma_{0max}$ between SFC 10 and 50%. It may be that fat crystals that protrude through the oil–water interface promote the fat particle adsorption either to the air–water interface directly or to already-adsorbed fat particles.

The E'_{max} of Cream B and Cream C increased when the SFC in the fat particles was between 10 and 50% (Fig. 4-7(b)). This finding suggests that adsorbed fat particles with appropriate SFC, build up the interfacial structure at the air–water interface via partial coalescence. In contrast, a similar relationship was not well-defined for Cream A, for which E'_{max} at 40 °C (SFC 12.6%) was 19.8 mN m^{-1}. Although the SFC value was in the 10–50% range, the E'_{max} value was not substantially higher than that of sodium caseinate at 40 °C (15.8±0.7 mN m^{-1}). The $\Delta\gamma_{0max}$ values at 10, 20, 30 and 40 °C were 1.06±0.27, 1.05±0.20, 1.53±0.30 and 3.30±0.68 mN m^{-1} s^{-1}, respectively (Table 4-1). Thus, sodium caseinate adsorbs faster at 40 °C than between 10 and 30 °C. When a fat particle approached the air–water interface, the interface had already been occupied by sufficient sodium caseinate to form a densely packed interfacial layer. Such a densely packed layer of sodium caseinate may prevent any further adsorption of Cream A to the air–water interface, even if it presents an appropriate SFC content, for example, 12.6%.

4.3.3. Interfacial structure of air–water interface

Fig. 4-8 shows the microscopy images of the air–water interfacial structures of sodium caseinate solution and the three creams after whipping. Fig. 4-8(a) is the interfacial structure with 2% w/w sodium caseinate solution in the absence of fat

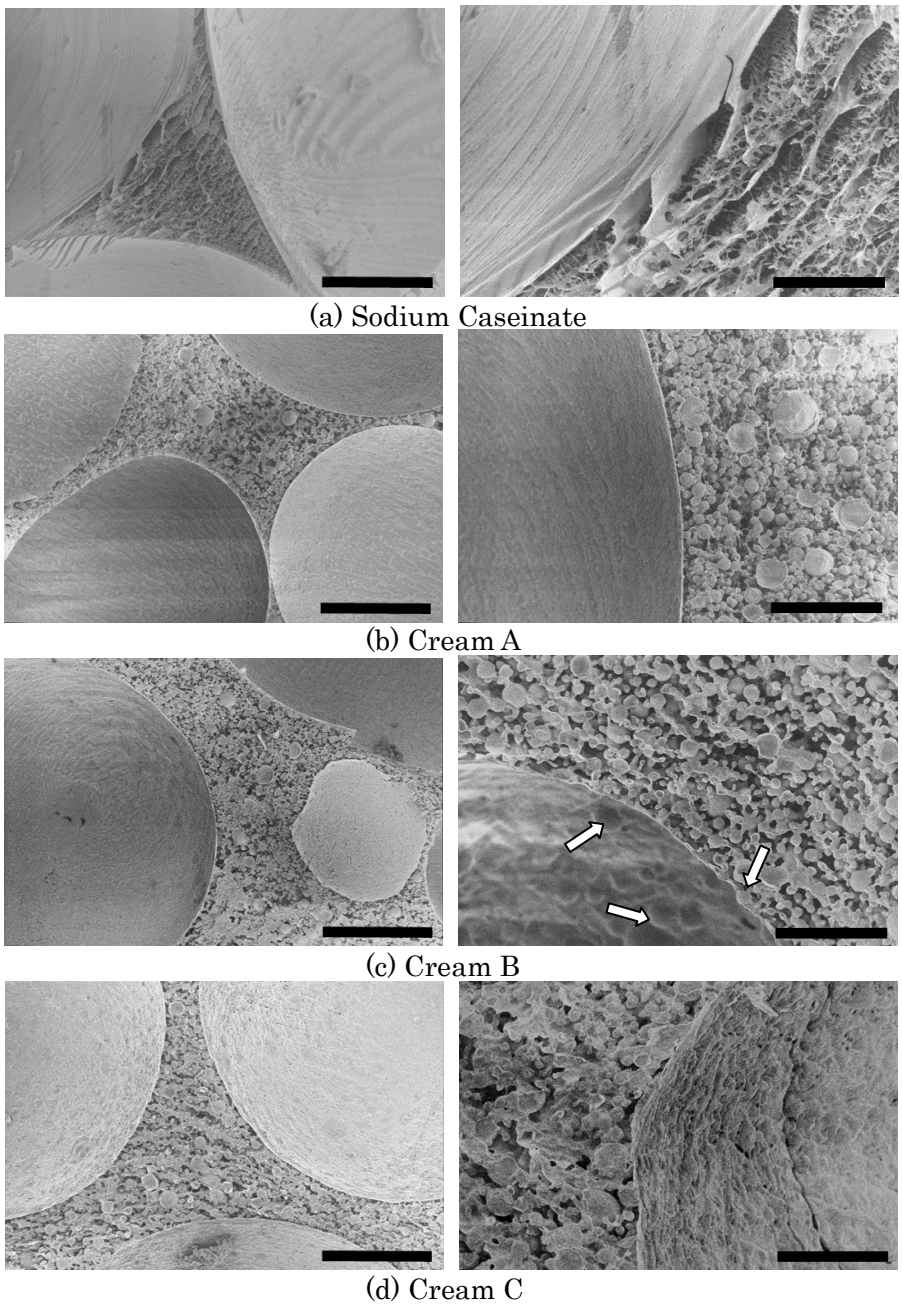

Fig. 4-8. Microstructures of air–water interfaces of whipped sodium caseinate solution and creams containing 40% w/w fat: (a) 2% w/w sodium caseinate; (b) Cream A; (c) Cream B; (d) Cream C. For the left column, magnification was ×1,000, and size bars in the photos show 30 μm; For the right column, magnification was ×3,000, and size bars in the photos show 10 μm. The arrows indicate the fat globules at the air–water interface.

particles. The large spherical vacant spaces are air bubbles, and the lamellar structures in the water phase are milk proteins concentrated by ice, as a result of the sample preparation for the microstructure observation by cryo-SEM. The air–water interface was very smooth and covered with sodium caseinate. In the interfacial structure of whipped Cream A (Fig. 4-8(b)), fat particles were observed, mainly in the water phase and seemed not to be attached to the air–water interface. The air–water interface structure exhibited a smooth surface, similar to that formed by sodium caseinate (Fig. 4-8(a)). Visualisation of the interfacial structure of whipped Cream B (Fig. 4-8(c)) indicated some fat globules at the air–water interface. These fat globules were ca. 2.0 μm, similar to those measured by the laser diffraction particle size analyser (1.7 μm). Thus, these data suggest that fat particles in Cream B can adsorb at the air–water interface without changing the original spheroidal shapes. Observation of the interfacial structure of whipped Cream C (Fig. 4-8(d)), identified fat particles adsorbed onto the air–water interface after whipping. Fat particles in whipped Cream C were more aggregated at the interface layer and in the water phase compared to those in Cream B. It was therefore difficult to discern any spheroidal fat particles that may have been present at the air–water interface.

These observed interfacial structures may be related to the interfacial rheology measurements. The $\Delta\gamma_{max}/\Delta\gamma_{0max}$ of Cream A at 10 °C was less than 1 (Fig. 4-7(a)). E'_{max} of diluted 40% w/w Cream A at 10 °C was 21.3±2.2 mN m^{-1} (Fig. 4-6 and Fig. 4-7(b)), which was almost the same as that of diluted 2% w/w sodium caseinate solution (21.9±4.4 mN m^{-1}) (Fig. 4-6). These results suggest that fat particles whose SFC was 100.0% did not adsorb onto the air–water interface to form an adsorbed layer with high mechanical strength. This speculation can be supported by the smooth surface of air bubbles observed in both the sodium caseinate solution (Fig. 4-7(a)) and Cream A (Fig. 4-7(b)). Similar results in protein–polysaccharide mixtures have been reported by Hanazawa and Murray (2013). They prepared sodium caseinate and xanthan mixtures

and investigated the effects of oil droplets on phase separation behaviour into the protein-rich and polysaccharide-rich phases. The highest inhibition behaviour of oil droplets to the phase separation was observed when the droplets were composed of 50% w/w solid oil (eicosane) and 50% w/w liquid oil (*n*-tetradecane), but the effect was not confirmed by the droplets composed of 100% w/w solid oil.

Compared to the sodium caseinate solution, the 40% w/w Cream B had a much larger E'_{max} of 27.0±4.8 mN m^{-1} at 10 °C (Fig. 4-6 and Fig. 4-7(b)). As shown in Fig. 4-8(c), partial coalescence occurred to a certain extent at the air–water interface while the fat particles adsorbed into the air–water interface. For 40% w/w Cream C, E'_{max} reached a maximum at 10 °C (34.0±2.0 mN m^{-1}, Fig. 4-6 and Fig. 4-7(b)). In addition, Fig. 4-7(a) suggests that fat particles of Cream C can adsorb faster than those of Cream A and Cream B at 10 °C, as discussed above. These behaviours of Cream C corresponded to its air–water interface microstructure (Fig. 4-8(d)), in which fat particles aggregated via partial coalescence at the air–water interface, causing high bubble stability.

References

Anderson, M., & Brooker, B. E. (1988). Dairy Foams. In E. Dickinson & G. Stainsby, (Eds.), *Advances in food emulsions and foams*. (Chapter 5, pp. 221–255). London, UK: Elsevier Applied Science.

Benjamins, J., Cagna, A., & Lucassen-Reynders, E. H. (1996). Viscoelastic properties of triacylglycerol/water interfaces covered by proteins. *Colloids and Surfaces A: Physicochemical and Engineering Aspects, 114,* 245–254.

Benjamins, J., Lyklema, J., & Lucassen-Reynders, E. H. (2006). Compression/expansion rheology of oil/water interfaces with adsorbed proteins. Comparison with the air/water surface. *Langmuir, 22,* 6181–6188.

Besner, H., & Kessler, H. G. (1998). Interfacial interaction during the foaming of nonhomogenized cream. *Milchwissenschaft, 53,* 682–686.

Boode, K., & Walstra, P. (1993) Kinetics of partial coalescence in oil-in-water emulsions. In E. Dickinson & P. Walstra, (Eds.), *Food colloids and polymers: Stability and mechanical properties*. (pp. 23–30). Cambridge, UK: Royal Society of Chemistry.

Brooker, B. E., Anderson, M., & Andrews, A. T. (1986). The development of structure in whipped cream. *Food Microstructure, 5,* 277–285.

Burke, J., Cox, A., Petkov, J., & Murray, B. S. (2014). Interfacial rheology and stability of air bubbles stabilized by mixtures of hydrophobin and β-casein. *Food Hydrocolloids, 34,* 119–127.

Chen, M., Sala, G., Meinders, M. B. J., van Valenberg, H. J. F., van der Linden, E., & Sagis, L. M. C. (2017). Interfacial properties, thin film stability and foam stability of casein micelle dispersions. *Colloids and Surfaces B: Biointerfaces, 149,* 56–63.

Cheng, H.-L., & Velankar, S. S. (2009). Controlled jamming of particle-laden interfaces using a spinning drop tensiometer. *Langmuir, 25,* 4412−4420.

Courthaudon, J.-L., Dickinson, E., & Dalgleish, D. G. (1991). Competitive adsorption of β-casein and nonionic surfactants in oil-in-water emulsions. *Journal of Colloid and Interface Science, 145,* 390–395.

Dalgleish, D. G. (1997). Structure–function relationships of caseins. In S. Damodaran & A. Paraf, (Eds)*, Food proteins and their applications.* (pp. 199–223). New York: Marcel Decker.

Davies, E., Dickinson, E., & Bee, R. (2000). Shear stability of sodium caseinate emulsions containing monoglyceride and triglyceride crystals. *Food Hydrocolloids, 14,* 145–153.

Dickinson, E. (1992). *An introduction to food colloids*. Oxford, UK: Oxford University Press.

Dickinson, E., & Iveson, G. (1993). Adsorbed films of β-lactoglobulin + lecithin at the hydrocarbon–water and triglyceride–water interfaces. *Food Hydrocolloids, 6,* 533–541.

Dickinson, E., Murray, B. S., & Stainsby, G. (1985). Time-dependent surface viscosity of adsorbed films of casein + gelatin at the oil–water interface. *Journal of Colloid and Interface Science, 106,* 259–262.

Dickinson, E., Rolfe, S. E., & Dalgleish, D. G. (1990). Surface shear viscometry as a probe of protein–protein interactions in mixed milk protein films adsorbed at the oil–water interface. *International Journal of Biological Macromolecules, 12,* 189–194.

Fredrick, E., Heyman, B., Moens, K., Fischer, S., Verwijlen, T., Moldenaers, P., … & Dewettinck, K. (2013). Monoacylglycerols in dairy recombined cream: II. The effect on partial coalescence and whipping properties. *Food Research International, 51,* 936–945.

Fuentes-Prado, E., & Martínez-Padilla, L. P. (2014). Colloidal stability and dilatational rheology at the air–water interface of peptides derived from thermal-acidic treated

wheat gluten. *Food Hydrocolloids, 41,* 210–218.

Fuller, G. T., Considine, T., Golding, M., Matia-Merino, L., MacGibbon, A., & Gillies, G. (2015). Aggregation behavior of partially crystalline oil-in-water emulsions: Part I – Characterization under steady shear. *Food Hydrocolloids, 43,* 521–528.

Hanazawa, T., & Murray, B. S. (2013). Effect of oil droplets and their solid/liquid composition on the phase separation of protein–polysaccharide mixtures. *Langmuir, 29,* 9841–9848.

Hinrichs, J., & Kessler, H. G. (1997). Fat content of milk and cream and effects on fat globule stability. *Journal of Food Science, 62,* 992–995.

Hotrum, N. E., Cohen Stuart, M. A. C., van Vliet, T., Avino, S. F., & van Aken, G. A. (2005). Elucidating the relationship between the spreading coefficient, surface-mediated partial coalescence and the whipping time of artificial cream. *Colloids and Surfaces A: Physicochemical and Engineering Aspects, 260,* 71–78.

Hotrum, N. E., Cohen Stuart, M. A., van Vliet, T., & van Aken, G. A. (2003). Flow and fracture phenomena in adsorbed protein layers at the air/water interface in connection with spreading oil droplets. *Langmuir, 19,* 10210–10216.

Hotrum, N. E., Cohen Stuart, M. A., van Vliet, T., & van Aken, G. A. (2004). Spreading of partially crystallized oil droplets on an air/water interface. *Colloids and Surfaces A: Physicochemical and Engineering Aspects, 240,* 83–92.

Hotrum, N. E., van Vliet, T., Cohen Stuart, M. A., & van Aken, G. A. (2002). Monitoring entering and spreading of emulsion droplets at an expanding air/water interface: A novel technique. *Journal of Colloid and Interface Science, 247,* 125–131.

Jakubczyk, E. & Niranjan, K. (2006). Transient development of whipped cream properties. *Journal of Food Engineering, 77,* 79–83.

Jara, F. L., Sánchez, C. C., Patino, J. M. R., & Pilosof, A. M. R. (2014). Competitive adsorption behavior of β-lactoglobulin, α-lactalbumin, bovine serum albumin in presence of hydroxypropylmethylcellulose. Influence of pH. *Food Hydrocolloids, 35,*

189–197.

Li, W., Wang, Y., Zhoa, H., He, Z., Zeng, M., Qin, F., & Chen, J. (2018). Effects of soluble soy polysaccharides and gum arabic on the interfacial shear rheology of soy β-conglycinin at the air/water and oil/water interfaces. *Food Hydrocolloids, 76,* 123–130.

Mezdour, S., Desplanques, S., & Relkin, P. (2011). Effects of residual phospholipids on surface properties of a soft-refined sunflower oil: Application to stabilization of sauce-types' emulsions. *Food Hydrocolloids, 25,* 613–619.

Murray, B. S., Færgemand, M., Trotereau, M., & Ventura, A. (1999). Comparison of the dynamic behaviour of protein films at the air–water and oil–water interfaces. In E. Dickinson & J. M. R. Patino (Eds.)*, Food emulsions and foams: Interfaces, interactions and stability.* (pp. 223–235). Cambridge, UK: Royal Society of Chemistry.

Murray, B. S., Dickinson, E., & Wang, Y. (2009). Bubble stability in the presence of oil-in-water emulsion droplets: Influence of surface shear versus dilatational rheology. *Food Hydrocolloids, 23,* 1198−1208.

Mutoh, T.-A., Nakagawa, S., Noda, M., Shiinoki, Y., & Matsumura, Y. (2001). Relationship between characteristics of oil droplets and solidification of thermally treated cream. *Journal of the American Oil Chemists' Society, 78,* 177–183.

Needs, E. C., & Huitson, A. (1991). The contribution of milk serum-proteins to the development of whipped cream structure. *Food Structure, 10,* 353–360.

Noda, M., & Shiinoki, Y. (1986). Microstructure and rheological behavior of whipping cream. *Journal of Texture Studies, 17,* 189–204.

Noskov, B. A., Latnikova, A. V., Lin, S.-Y., Loglio, G., & Miller, R. (2007). Dynamic surface elasticity of β-casein solutions during adsorption. *Journal of Physical Chemistry C, 111,* 16895–16901.

Peng, D., Jin, W., Tang, C., Lu, Y., Wang, W., Li, J., & Li, B. (2018). Foaming and

surface properties of gliadin nanoparticles: Influence of pH and heating temperature. *Food Hydrocolloids, 77,* 107–116.

Ridout, M. J., Mackie, A. R., & Wilde, P. J. (2004). Rheology of mixed β-casein/β-lactoglobulin films at the air–water interface. *Journal of Agricultural and Food Chemistry, 52,* 3930–3937.

Tamm, F., & Drusch, S. (2017). Impact of enzymatic hydrolysis on the interfacial rheology of whey protein/pectin interfacial layers at the oil/water-interface. *Food Hydrocolloids, 63,* 8–18.

Van Aken, G. A. (2001). Aeration of emulsions by whipping. *Colloids and Surfaces A: Physicochemical and Engineering Aspects, 190,* 333–354.

Walstra, P., Wouters, J. T. M., & Geurts, T. J. (2006). *Dairy science and technology*. (2nd ed.). Boca Raton: CRC Press.

Wouters, A. G. B., Rombouts, I., Fierens, E., Brijs, K., Blecker, C., Delcour, J. A., & Murray, B. S. (2018). Foaming and air–water interfacial characteristics of solutions containing both gluten hydrolysate and egg white protein. *Food Hydrocolloids, 77,* 176–186.

Chapter 5

Summary

Chapter 2:

A model system consisting of sodium caseinate (SC) + xanthan ± a low volume fraction of oil-in-water emulsion droplets was studied. The phase separation behaviour of xanthan + sodium caseinate was investigated as function of these two variables, followed by experiments on the same systems where oil droplets were introduced. More than 20 mM calcium ion concentration ([Ca^{2+}]) was needed to induce phase separation at pH 6.4 and 5.9, but at pH 5.4, phase separation occurred at as low as 5 mM [Ca^{2+}] and a lower concentration of SC or xanthan was required to induce phase separation. An increase in size of sodium caseinate aggregates is proposed as the main factor promoting phase separation. When oil droplets stabilized by sodium caseinate were added to systems containing 0.05–0.1% w/w xanthan at pH 6.4 this appeared to inhibit significantly the phase separation of the mixtures at [Ca^{2+}] = 22 mM. Simple calculations showed that this effect cannot reasonably be due to excessive accumulation of protein at the droplet surfaces, which is then carried away by the droplets due to creaming. Consequently, a possible mechanism of the inhibition is accumulation of droplets at and strengthening of, the water–water interface of the caseinate–xanthan phase separating entities

Chapter 3:

The phase separation of a model system consisting of sodium caseinate + xanthan ± a low fraction (up to 3% w/w) of an oil-in-water emulsion was studied at room temperature (20−25 °C). The composition of the oil phase was either 100% w/w

n-tetradecane (TD); 50% w/w TD + 50% w/w eicosane (EC) or 100% w/w EC. The droplets in these three "emulsions" were therefore totally liquid, partially solid, and totally solid, respectively. In the presence of 22 mM calcium ion concentration ($[Ca^{2+}]$), the mixed TD+EC droplets were most effective at inhibiting phase separation, while the EC emulsions could not prevent phase separation at all. At 32 mM $[Ca^{2+}]$ the emulsions tended to promote phase separation, possibly due to enhanced calcium ion-induced droplet aggregation. The apparent interfacial viscosity (η_i) between two macroscopically separated phases was also measured. In the presence of the semisolid mixed droplets η_i = 25 mN s m^{-1}, significantly higher than η_i with the pure (liquid) TD droplets (15 mN s m^{-1}) or with the pure solid EC droplets (12 mN s m^{-1}) or in the absence of droplets (<3 mN s m^{-1}). Confocal microscopy showed that the microstructure of the phase separating regions also depended upon the composition of the oil droplets, and it is tentatively suggested that the more marked effects of the mixed emulsion droplets were due to them forming a stronger network at the interface via partial coalescence. Control of the extent of interfacial aggregation of droplets is therefore possibly one way to influence the course of phase separation in biopolymer mixtures.

Chapter 4:

The role of solid fat content (SFC) within fat particles was examined for its effects on adsorption behaviour at the air–water interface. Three kinds of vegetable oil with different SFC profiles were mixed with a sodium caseinate solution (2% w/w) to prepare the creams, whose fat contents were adjusted in the range of 0–40% w/w. The decrease of interfacial tension at the air–water interface was measured for creams and the sodium caseinate solution, and the ratio of the maximum decrease rate of creams ($\Delta\gamma_{max}$)-to-the sodium caseinate solution ($\Delta\gamma_{0max}$), $\Delta\gamma_{max}/\Delta\gamma_{0max}$, was calculated. The interfacial elastic modulus (E') of creams and sodium caseinate solution was also measured and found to initially increase with time but decreased after the maximum

value (E'_{max}). Both $\Delta\gamma_{max}/\Delta\gamma_{0max}$ and E'_{max} were affected by the temperature, fat content of creams and SFC in fat particles. The largest increase for $\Delta\gamma_{max}/\Delta\gamma_{0max}$ and E'_{max} was observed when the SFC of creams was between 10 and 50% w/w. The microscopic structures of the air–water interface of creams after whipping were also affected by the SFC, such that fat particles containing 28.4% SFC were found to adsorb and aggregate at the air–water interface layer. These results suggest that the adsorption of fat particles onto the air–water interface and interfacial structure formation by adsorbed fat particles were promoted via partial coalescence.

Acknowledgements

First of all, I would like to thank Dr. Yasuki Matsumura, Professor of Graduate School of Agriculture, Kyoto University, for his constructive advice and invaluable discussion for this thesis. I am grateful to Dr. Brent S. Murray, Professor of School of Food Science and Nutrition, University of Leeds, for his helpful discussion and support for my research, and Dr. Kentaro Matsumiya and all members of Laboratory of Quality Analysis and Assessment, Graduate School of Agriculture, Kyoto University, for their warm support.

I would also like to thank Dr. Yoshihiro Kawasaki, Senior Managing Director of Megmilk Snow Brand., Ltd., Mr. Mototake Murakami, General Manager of R&D Planning Dept., Mr. Hitoshi Hatamoto, General Manager of Products Development Dept., Mr. Atsushi Serizawa, General Manager of Milk Science Instistute, Dr. Takashi Fujita, previous General Manager of Milk Science Instistute, and Dr. Yasuhiko Shiinoki, former General Manager of Milk Science Instistute and Dr. Taka-aki Mutoh, Manager of Corporate Planning Division who gave me warm encouragemnent and helpful advice.

Finally, I am thankful to my colleagues and my family for their everyday warm support.

List of Publications

Hanazawa, T. & Murray, B. S. (2014). The influence of oil droplets on the phase separation of protein–polysaccharide mixtures. *Food Hydrocolloids*, **34**, 128-137

Hanazawa, T. & Murray, B. S. (2013). Effect of oil droplets and their soild/liquid composition on the phase separation of protein–polysaccharide mixtures. *Langmuir*, **29**, 9841-9848

Hanazawa, T., Sakurai, Y., Matsumiya, K., Mutoh, T., & Matsumura, Y. (2018). Effects of solid fat content in fat particles on their adsorption at the air–water interface. *Food Hydrocolloids*, **83**, 317-325